

Main Line Fault Localization Methodology in Smart Grid – Part 2: Extended TM2 Method, Measurement Differences and L1 Piecewise Monotonic Data Approximation for the Overhead Medium-Voltage Broadband over Power Lines Networks Case

Athanasios G. Lazaropoulos¹

1: School of Electrical and Computer Engineering / National Technical University of Athens / 9 Iroon Polytechniou Street / Zografou, GR 15780

Received June 13, 2017; Accepted September 2, 2017; Published October 2, 2017

Enriching the fault identification methodology of the first paper, this second paper investigates the performance of the identification of main distribution line faults when broadband over power lines (BPL) networks are deployed. The main issue that is concerned in this paper is the impact of measurement differences on the fault identification process performance.

The main contribution of this paper, which is focused on the identification of the main distribution line faults when measurement differences occur, is the application of the L1 piecewise monotonic data approximation (L1PMA) in order to cope with the measurement differences that influence the reflection coefficients derived from the extended TM2 method. Through the L1PMA application, measurement differences are confronted in order to prevent the trigger of a false alarm about the existence of a main distribution line fault. The combined operation of the extended TM2 method and L1PMA concludes the introductory phase (fault identification) of the main line fault localization methodology (MLFLM).

Keywords: Smart Grid; Intelligent Energy Systems; Broadband over Power Lines (BPL) Networks; Power Line Communications (PLC); Faults; Fault Analysis; Fault Localization; Distribution Power Grids

1. Introduction

The need for more intelligent, stable and autonomous transmission and distribution power grids is met by the deployment of the smart grid package, which comprises both hardware and software proposals, across the entire vintage power grid infrastructure [1]-[4]. As concerns the smart grid hardware, broadband over power lines (BPL) networks have rightfully attracted the attention among the available wired and wireless communications media, which anyway may interoperate in the smart grid environment [5]-[7]. A major advantage of the BPL networks is the fact that their deployment is based on the already existent power grid equipment devoted to transfer and deliver power. As concerns the smart grid software, a myriad of smart grid applications

can be supported by all the available wired and wireless communication solutions of smart grid, including BPL technology, since the traditional power grid can be further treated as an integrated intelligent IP-based network environment [2], [8]-[10].

As concerns the determination of the channel attenuation and reflection coefficient of overhead medium-voltage (OV MV) BPL networks, the well-established hybrid method, which consists of [6], [10]-[26]: (i) a bottom-up approach that is based on the multiconductor transmission line (MTL) theory, eigenvalue decomposition (EVD) and singular value decomposition (SVD); and (ii) a top-down approach that is denoted as TM2 method and is based on the concatenation of multidimensional chain scattering matrices. In accordance with [1], original TM2 method gives as outputs the corresponding transfer function and reflection coefficients for the normal operation of OV MV BPL networks whereas extended TM2 method gives as output the reflection coefficients for the operation where a main distribution line fault occurs (fault operation). In fact, the main distribution line fault subcategory forms the only fault case which cannot be treated by the available tools for identifying and localizing faults and instabilities, say Topology Identification Methodology (TIM) and Fault and Instability Identification Methodology (FIIM) of [3], [4]. The identification of main distribution line faults is going to be treated by the approach of reflection coefficients of the extended TM2 method, which has initially been presented in [1]. As presented in [1], the comparison of the reflection coefficients between the normal operation, as given by the original TM2 method, and the fault operation, as determined by the extended TM2 method, defines the existence of main distribution line faults.

As already been mentioned in [3], [4], [6], [10], [26], measurement differences between the experimental and theoretical results occur during the transfer function determination of OV MV BPL topologies because of a number of practical reasons and “real-life” conditions. Similar measurement differences also occur during the determination of reflection coefficients. Following the same methodology to counteract the measurement differences of reflection coefficients with those of transfer functions, piecewise monotonic data approximations (PMAs), such as L1PMA, L2WPMA and L2CXCVCV, are also applied to the reflection coefficient measurements in order to restore the theoretical reflection coefficient [3], [4], [6], [10], [26]. Among the available PMAs that have been applied to BPL networks, L1PMA, which has been thoroughly analyzed and assessed in [3], [26], is selected to be applied to the restoration of theoretical values of reflection coefficients. In this paper, the performance of L1PMA is assessed when various intensities of measurement differences are considered regardless of the examined OV MV BPL topology and the nature of the terminal load. Synoptically, the primary objective of this paper is to identify the main distribution line faults even if measurement differences occur while the fault alarm can be prevented due to the measurement differences.

The rest of this paper is organized as follows: In Sec.II, the findings of [1] that are used in this paper are briefly outlined. In Sec.III, a brief presentation of the measurement differences in BPL networks and L1PMA is given. Also, the suitable performance metrics for assessing the mitigation against measurement differences and for identifying a main distribution line fault are demonstrated. Sec.IV discusses the simulations of various OV MV BPL networks intending to mark out the mitigation performance of L1PMA against measurement differences during the main distribution line fault identification. Sec.V concludes this paper.

2. Brief Presentation of the OV MV MTL Configurations, OV MV BPL Topologies, Hybrid Method and the Main Distribution Line Faults

In accordance with [1], the OV MV MTL configuration, which is used in these three papers, is presented in Fig. 1(a) of [26] while its structure properties concerning the number of phase lines, the phase line spacings and the configuration heights are reported in [12], [13], [19], [21], [23], [27]-[29]. As the ground properties are considered, the impact of imperfect ground on broadband signal propagation and transmission via OV MV MTL configurations is analyzed in [12], [13], [19], [21], [23], [30]-[32].

According to [1], OV MV BPL networks are divided into cascaded OV MV BPL topologies. These OV MV BPL topologies are characterized by average path lengths of the order of 1000m which are bounded by BPL repeaters. With reference to Fig. 1(a) of [1], a typical OV MV BPL topology is presented while four indicative OV MV BPL topologies of average path length are defined and examined in these three papers. The topological specifications of the four indicative OV MV BPL topologies are detailed in [1] in order to describe respective typical urban, suburban, rural and “LOS” cases. Certain assumptions for the circuital parameters of OV MV BPL topologies, which are required by the hybrid method, are also given in [1].

Similarly to [1], [11]-[25], [31]-[33], the well-established hybrid method is applied in these three papers. More analytically, the hybrid method consists of: (i) a bottom-up approach that is based on the MTL theory, EVD and SVD decomposition; and (ii) a top-down approach that further comprises either the original TM2 method for the normal operation or the extended TM2 method for the main distribution line fault operation. The output of the hybrid method, which is the EVD modal reflection coefficient matrix $\Gamma_{in}^m \{ \}$, is further processed by the coupling scheme module that determines the practical way of the BPL signal injection into OV MV lines. In the case of Wire-to-Ground (WtG) coupling schemes, which are examined in these papers, the WtG coupling reflection coefficient $\Gamma^{WtG} \{ \}$ is determined by [1]

$$\Gamma^{WtG} \{ \} = \left[\mathbf{C}^{WtG} \right]^T \cdot \mathbf{T}_V \cdot \Gamma_{in}^m \{ \} \cdot \mathbf{T}_V^{-1} \cdot \mathbf{C}^{WtG} \quad (2)$$

where \mathbf{C}^{WtG} is the coupling column vector and \mathbf{T}_V is a matrix that depends on the frequency, the OV MV MTL configuration and the physical properties of the cables.

Already been mentioned in [1], critical problematic conditions can occur across the distribution power grid during its continuous normal operation. These problematic conditions differ from the measurement differences and can be divided into two categories, namely: faults and instabilities [3]-[6], [10]. Main distribution line faults, which are examined in these three papers, define a subcategory of the fault operation and describe the condition where a main distribution line is interrupted due to physical or human reasons [5]. Depending on the location of the conductors of the main distribution lines after the fault, main distribution line faults can be assumed to behave as either short- or open-circuit terminal loads whether the lines lie in the air or on the ground, respectively.

3. Measurement Differences, Presentation of L1PMA and Performance Metric

Apart from the faults and instabilities that cause critical damages to the transmission and distribution power grid infrastructure, a set of practical reasons and “real-life” conditions create significant differences between experimental measurements and theoretical results during the various determinations relating with the BPL networks. In accordance with [6], the set of measurement difference causes can be grouped into six categories, namely: (i) Isolation difficulties of specific MTL parameters in time- and frequency-domain; (ii) Low accuracy and sensitivity of the used equipment during measurements; (iii) Cross-talk and resonant phenomena due to the parasitic capacitances and inductances of lines; (iv) The weakness of including specific wiring and grounding practices; (v) Practical impedance deviations of lines, branches, terminations and transmitting/receiving ends; and (vi) The isolation lack of the noise effect during the transfer function computations.

The acquired PMA experience in the case of BPL coupling transfer functions across transmission and distribution power grids is here extended in order to cope with the measurement differences that may be present during the measurement of reflection coefficients. In accordance with [3]-[6], [10], [26], PMAs are going to exploit their piecewise monotonicity property by decomposing the reflection coefficient data into separate monotonous data sections between adjacent turning points (primary extrema). Then, PMAs separately handle the monotonous sections by proposing suitable regression approximations. Similarly to the coupling transfer function case, L1PMA software is modified in order to receive as inputs the measured OV MV BPL reflection coefficient data (i.e., either from the original TM2 method or the extended TM2 method), the measurement frequencies and the number of monotonic sections (i.e., either user- or computer-defined) and give as outputs the optimal primary extrema and the best fit of the measured OV MV BPL reflection coefficient data. In mathematical terms and with reference to eq. (2), the measured OV MV BPL reflection coefficient $\overline{\Gamma^{\text{WtG}^s}}$ for given WtG^s coupling scheme is determined by

$$\overline{\Gamma^{\text{WtG}^s}}(f_i) = \Gamma^{\text{WtG}^s}(f_i) + e(f_i), i=1, \dots, u \quad (3)$$

where $f_i, i=1, \dots, u$ denotes the measurement frequency, $e(f_i)$ synopsis the total measurement difference due to the aforementioned six categories and u is the number of subchannels in the examined frequency range.

Generalizing eq. (3), the measured OV MV BPL reflection coefficient column vector $\overline{\Gamma^{\text{WtG}}}$ is then determined by

$$\overline{\Gamma^{\text{WtG}}} \equiv \overline{\Gamma^{\text{WtG}}}(\mathbf{f}) = \left[\overline{\Gamma^{\text{WtG}}}(f_1) \quad \dots \quad \overline{\Gamma^{\text{WtG}}}(f_i) \quad \dots \quad \overline{\Gamma^{\text{WtG}}}(f_u) \right]^T \quad (3)$$

where $\mathbf{f} = [f_1 \quad \dots \quad f_i \quad \dots \quad f_u]^T$ is the measurement frequency column vector.

Similarly to the measured OV MV BPL reflection coefficient column vector $\overline{\Gamma^{\text{WtG}}}$, the theoretical OV MV BPL reflection coefficient column vector Γ^{WtG} can also be defined. With reference to [26], the theoretical OV MV BPL reflection coefficient column vector, the measured OV MV BPL reflection coefficient column vector, the measurement frequency column vector and the number of monotonic sections are

received by the LIPMA software presented in [34]. LIPMA software processes its inputs and gives as outputs the approximated theoretical OV MV BPL reflection coefficient column vector $\overline{\Gamma}_{\text{theor}}^{\text{WtG}}$ and the approximated measured OV MV BPL reflection coefficient column vector $\overline{\Gamma}_{\text{meas}}^{\text{WtG}}$.

Similarly to the performance metric CSPpM of FIIM [5], the proposed main distribution line fault identification percentage metric (MDLFI), which acts as the accompanying performance metric of the identification of main distribution line faults when measurement differences occur, is given by

$$MDLFI = \frac{\sum_{k_{\text{sect}}=k_{\text{sect,min}}}^{k_{\text{sect,max}}} MDLFI_{\text{par}}(k_{\text{sect}})}{(k_{\text{sect,max}} - k_{\text{sect,min}} + 1) \times u} \quad (4)$$

where

$$MDLFI_{\text{par}}(k_{\text{sect}}) = \sum_{i=1}^u \frac{|\overline{\Gamma}_{\text{meas}}^{\text{WtG}}(f_i, k_{\text{sect}}) - \overline{\Gamma}_{\text{theor}}^{\text{WtG}}(f_i, k_{\text{sect}})|}{|\overline{\Gamma}_{\text{theor}}^{\text{WtG}}(f_i, k_{\text{sect}})|} \quad (5)$$

, $k_{\text{sect,min}}$ is the lower monotonic section bound, which is assumed to be equal to 1 in this paper, and $k_{\text{sect,max}}$ is the upper monotonic section bound, which is assumed to be equal to 20 in this paper. Overall, note that MDLFI describes the relative error between LIPMA approximations of the measured and theoretical data by receiving the arithmetic mean of its MDLFI_{par} components. The behavior of the aforementioned percentage metric is going to be examined in Sec.IV in comparison with the magnitude of the measurement differences while a critical threshold of the MDLFI (MDLFI_{thr}) that is going to act as the warning limit of a main distribution line fault is also analyzed. Relative decisions regarding the dependencies of MDLFI_{thr} on various parameters are also presented in Sec.IV.

4. Numerical Results and Discussion

4.1 Simulation Goals and Parameters

Various types of OV MV BPL topologies and measurement difference distributions are simulated with the purpose of evaluating the LIPMA mitigation performance against measurement differences and the accuracy of identifying a main distribution line fault when it occurs by eliminating the false alarm likelihood. Similarly to the measurement differences of OV MV BPL coupling transfer functions, the measurement differences that occur in OV MV BPL networks during the determination of reflection coefficients are typically described by continuous uniform distributions (CUDs) with range from 0 to a maximum CUD value that is equal to α_{MD} .

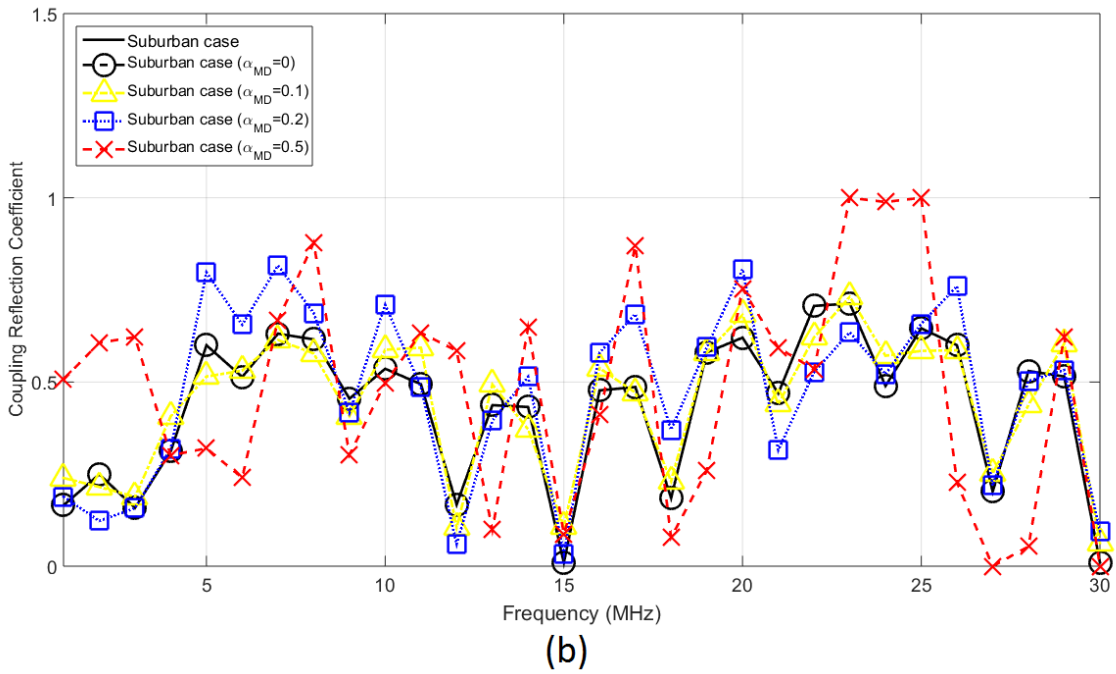
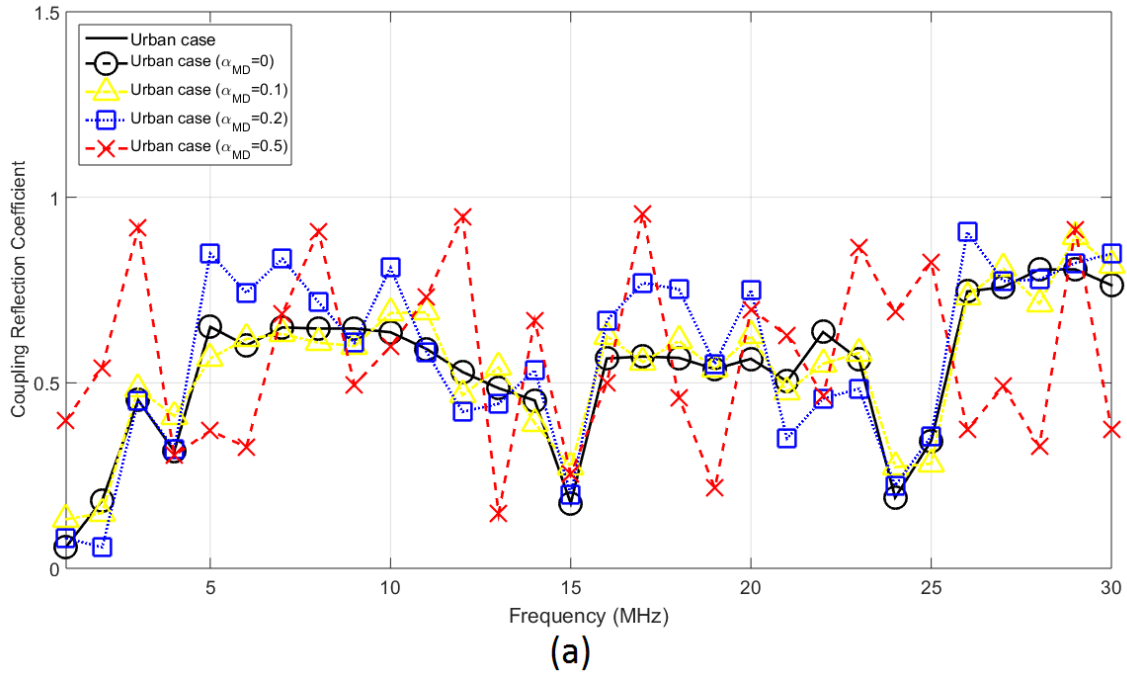
As regards the operation parameters of hybrid method and LIPMA, the BPL frequency range and the flat-fading subchannel frequency spacing are assumed equal to 1-30MHz and 1MHz, respectively. Therefore, the number of subchannels u in the examined frequency range is equal to 30. In accordance with [1], the WtG³ coupling scheme is applied during the following simulations. Finally, the maximum number of monotonic sections that is going to be used is assumed to be equal to 20 [26].

As the indicative OV MV BPL topologies are concerned, their topological characteristics concerning the number of branches, the length of main distribution lines and branches as well as the fault location have already been determined in [1].

4.2 Measurement Differences and Faults in Indicative OV MV BPL Topologies

Already been presented in [1], the main distribution line faults differentiate the reflection coefficient behavior between the normal and fault operation. Hence, significant differences occur between the theoretical and measured reflection coefficients. At the same time, there are also six categories, which have been reported in Sec.III, that may create additional measurement differences between the existing coupling reflection coefficients of the normal and fault operation for given OV MV BPL topology.

For comparison reasons only, the aforementioned four measurement difference distributions are first applied to the theoretical coupling reflection coefficients. In Figs. 1(a)-(d), the magnitude of the theoretical coupling reflection coefficients are plotted versus frequency for the four indicative OV MV BPL topologies –i.e., urban, suburban, rural and “LOS” case of Sec.2.2 of [1]–, respectively, when the four indicative measurement difference CUDs are applied for a given indicative OV MV BPL topology. Note that during the normal operation the terminal load is assumed to be matched to the characteristic impedance of the modal channels.



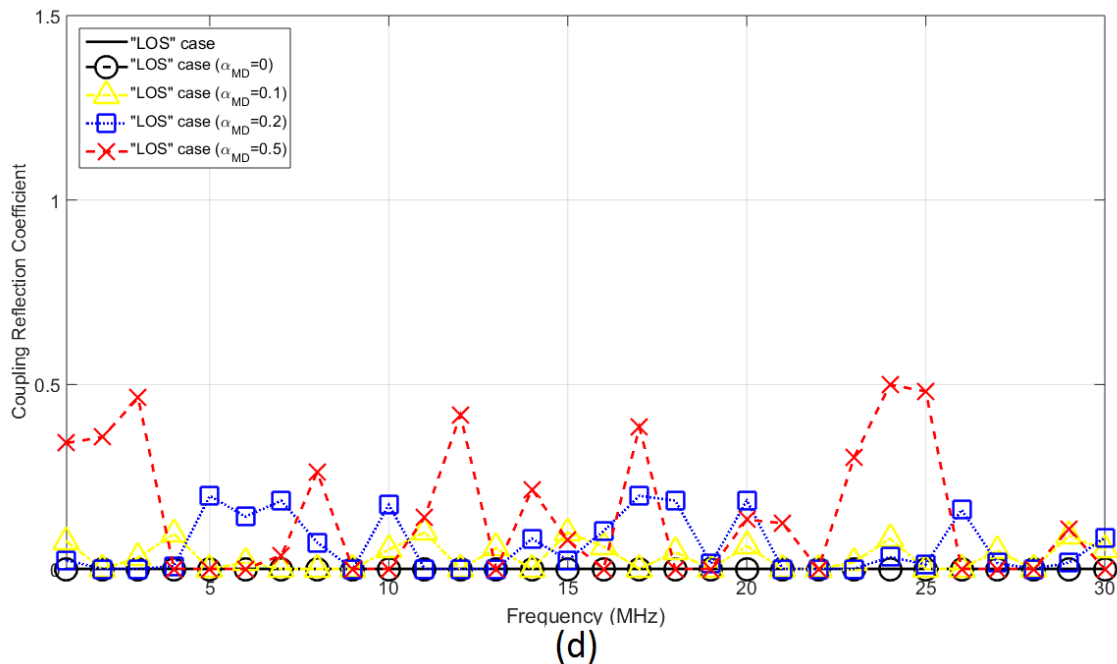
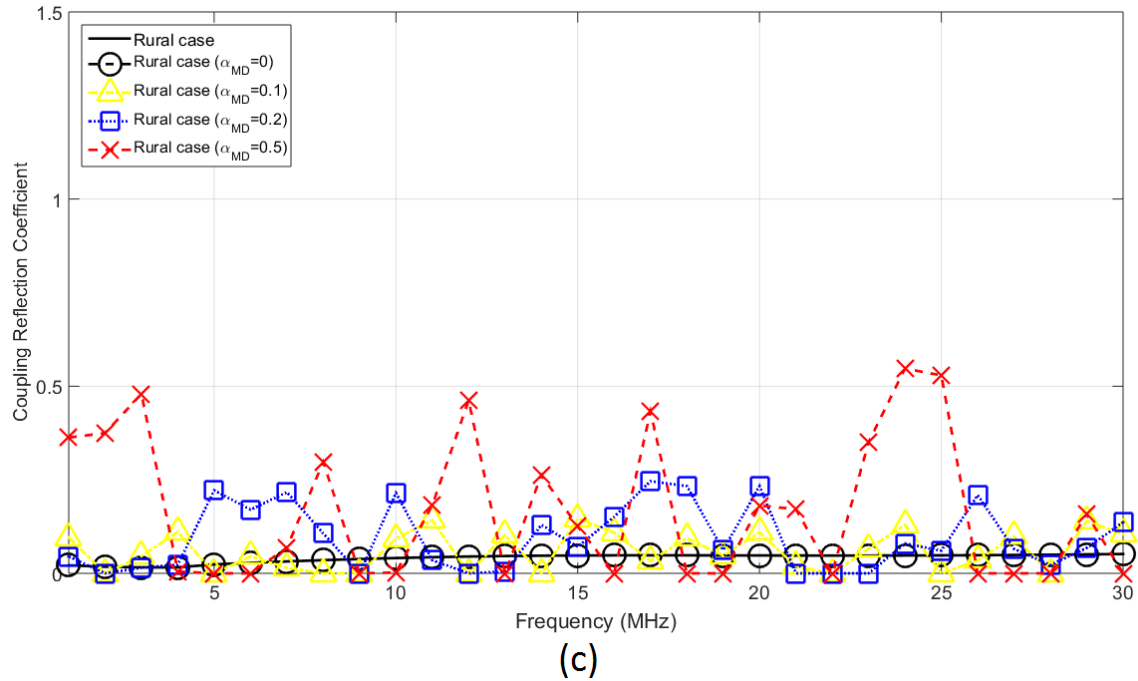
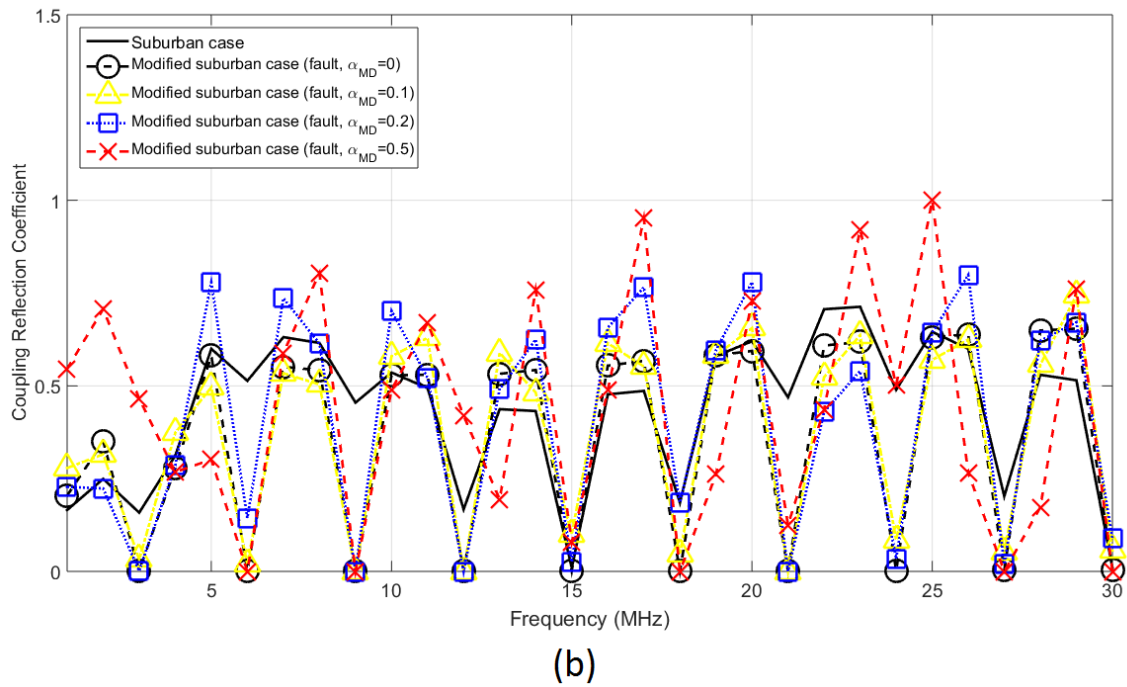
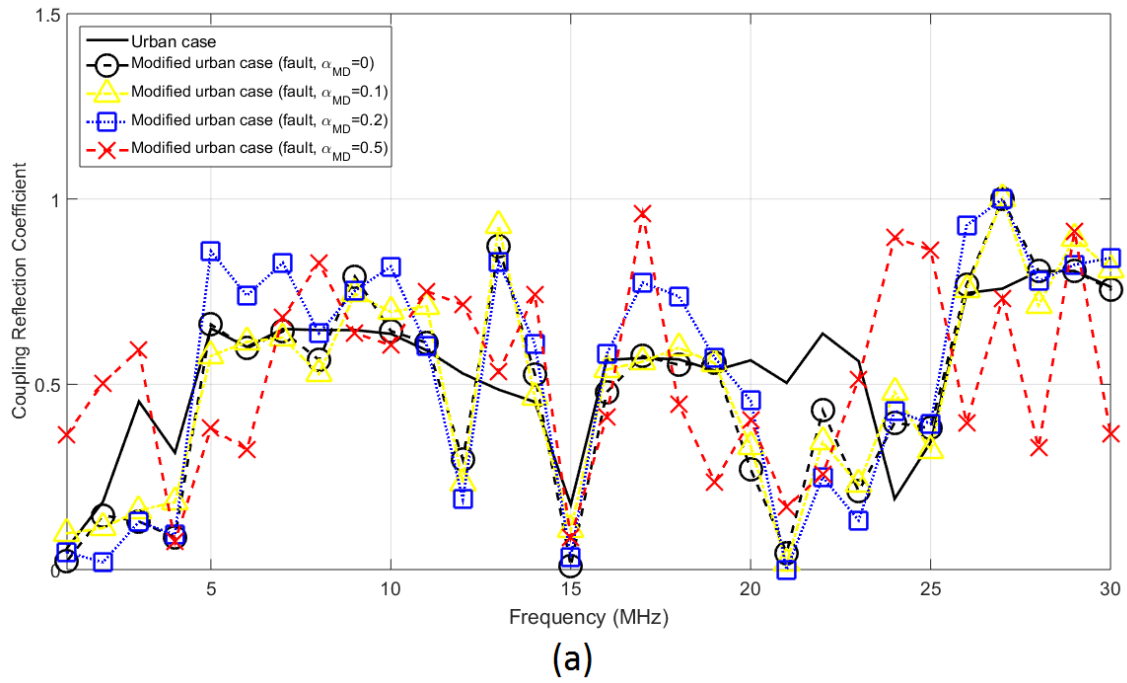


Figure 1. Magnitude of theoretical coupling reflection coefficients of OV MV BPL topologies contaminated by the four indicative measurement difference distributions ($CUD/a_{MD}=0$, $CUD/a_{MD}=0.1$, $CUD/a_{MD}=0.2$ and $CUD/a_{MD}=0.5$). (a) Urban case. (b) Suburban case. (c) Rural case. (d) “LOS” case.

The combined impact of the measurement differences and the main distribution line faults on the OV MV BPL coupling reflection coefficient is here investigated. More specifically, in Figs. 2(a)-(d), the theoretical coupling reflection coefficient is plotted versus frequency for the indicative OV MV BPL topologies, respectively –i.e., urban, suburban, rural and “LOS” case of Sec.2.2 of [1]–. In each figure,

the measured coupling reflection coefficient after the main distribution line fault at 750 m from the transmitting end is also given for the respective modified OV MV BPL topology –i.e., modified urban, suburban, rural and “LOS” case of Sec.4.3 of [1]– when measurement differences follow four indicative measurement difference distributions, namely: (i) CUD with $a_{MD}=0$ (no measurement differences); (ii) CUD with $a_{MD}=0.1$; (iii) CUD with $a_{MD}=0.2$; and (iv) CUD with $a_{MD}=0.5$. Similarly to [1], it should be noted that the magnitude of the OV MV BPL coupling reflection coefficients is demonstrated in the following figures of this paper while the terminal loads during the fault operation are assumed to be short-circuits in Figs. 2(a)-(d). In Figs. 3(a)-(d), same figures with Figs. 2(a)-(d) are shown but for the case of open-circuit terminal loads.



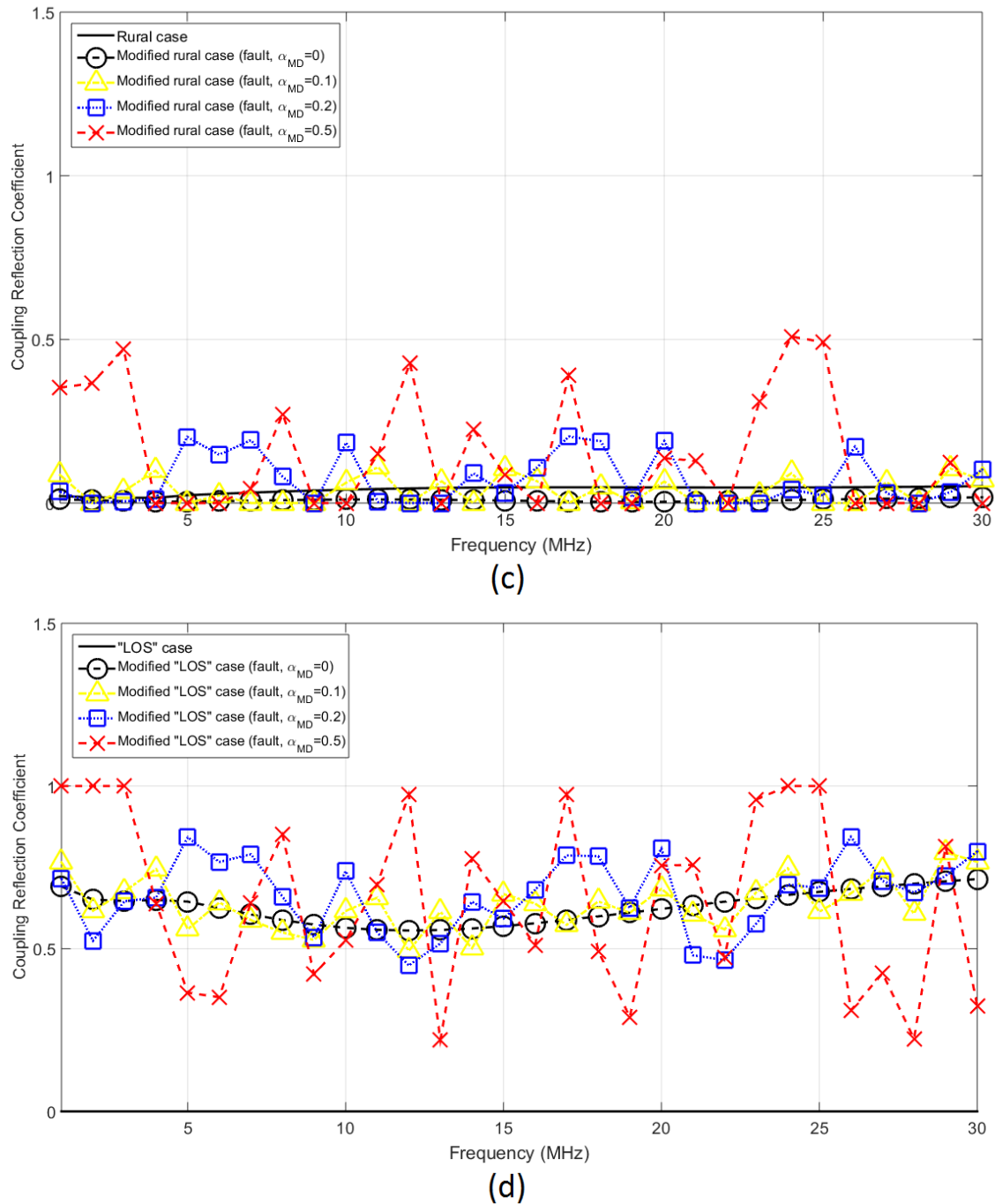
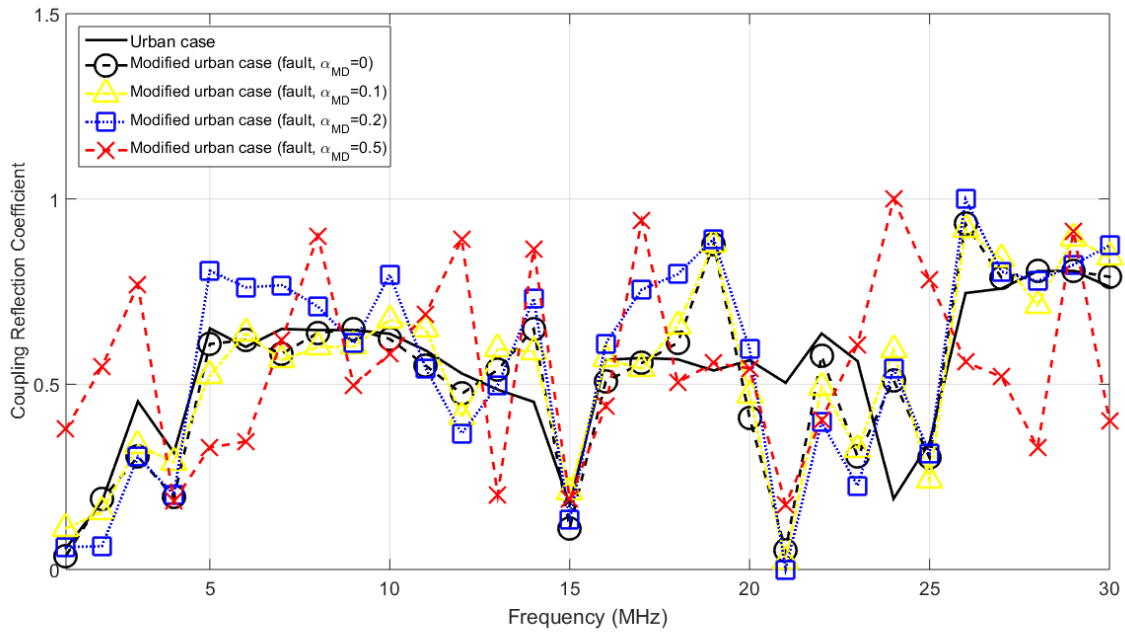
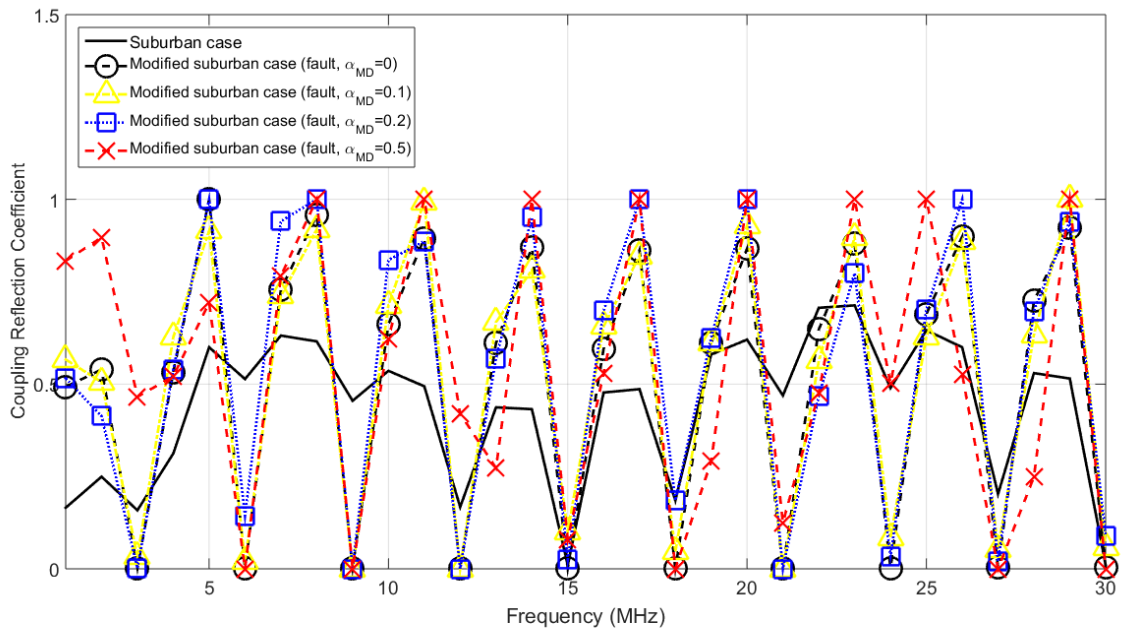


Figure 2. Theoretical and measured coupling reflection coefficients (measurement differences and main distribution line fault) of OV MV BPL topologies when four indicative measurement difference distributions ($CUD/a_{MD}=0$, $CUD/a_{MD}=0.1$, $CUD/a_{MD}=0.2$ and $CUD/a_{MD}=0.5$) are applied while the terminal load is assumed to be short-circuit. (a) Urban and modified urban case. (b) Suburban and modified suburban case. (c) Rural and modified rural case. (d) "LOS" and modified "LOS" case.



(a)



(b)

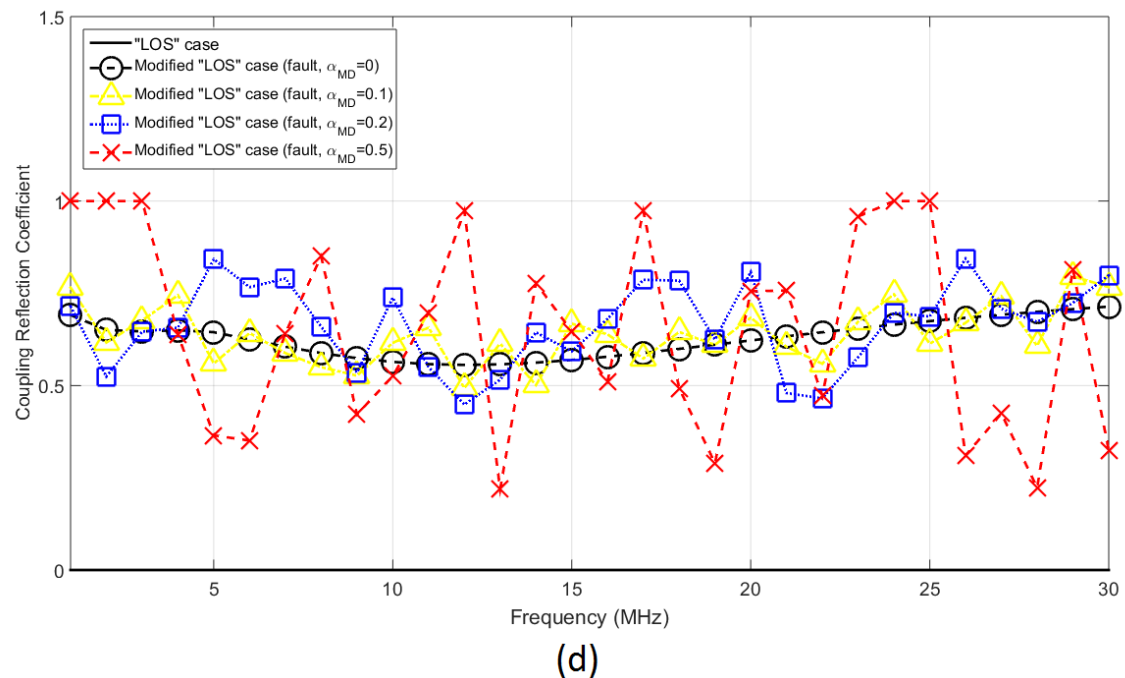
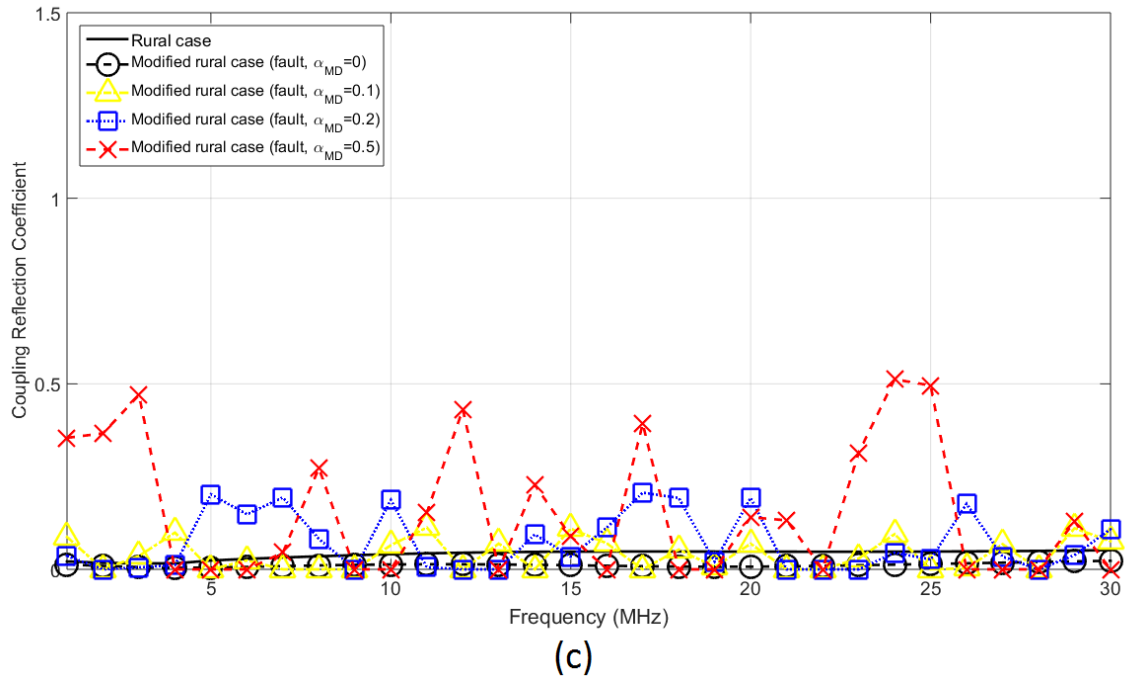


Figure 3. Same plots with Figure 2 but for open-circuit terminal loads during the fault operation.

Depending on the examined OV MV BPL topology, the notches of measurement differences incommode the identification of a main distribution line fault by creating different levels of difficulty. Observing Figs. 1(c) and 1(d), the OV MV BPL topologies of low number of branches, such as rural and "LOS" cases, are characterized by rare and shallow notches. When a main distribution line fault occurs, the coupling reflection coefficient curves of the fault operation significantly differ from the respective curves of the normal operation. The superimposed notches, which come from the measurement

differences, imply the presence of a main distribution line fault because the curves of the theoretical and measured reflection coefficients still significantly differ. Conversely, OV MV BPL topologies of high number of short branches maintain significant notches due to the multipath environment.

Already been mentioned in [1], the first sign of the presence of a main distribution line fault is the immediate communications failure between the transmitting and receiving end but it is not the only sign. From Figs. 2(a)-(d) and Figs. 3(a)-(d), it is evident that significant coupling reflection coefficient differences occur between the normal and fault operation even if measurement differences are neglected (i.e., $CUD/a_{MD}=0$). Regardless of the terminal load (i.e., short- or open-circuit terminations), when a main distribution line fault occurs, the superposition of the measurement differences to the reflection coefficients of the fault operation deteriorates the identification process of a main distribution line fault. In fact, as the maximum value a_{MD} of CUD increases so do the notches across the reflection coefficient curves.

Comparing Figs. 1(a) and 1(b) with Figs. 2(a), 2(b), 3(a) and 3(b), the coupling reflection coefficients of the fault operation satisfactorily differ from the ones of the normal operation when a main distribution line fault occurs. However, in the more aggravated OV MV BPL topologies, such as urban and suburban cases, the imposed notches of measurement differences are tangled with the notches of the coupling reflection coefficients. The plethora of notches creates confusion when a decision needs to be taken whether a noisy environment or main distribution line fault occurs.

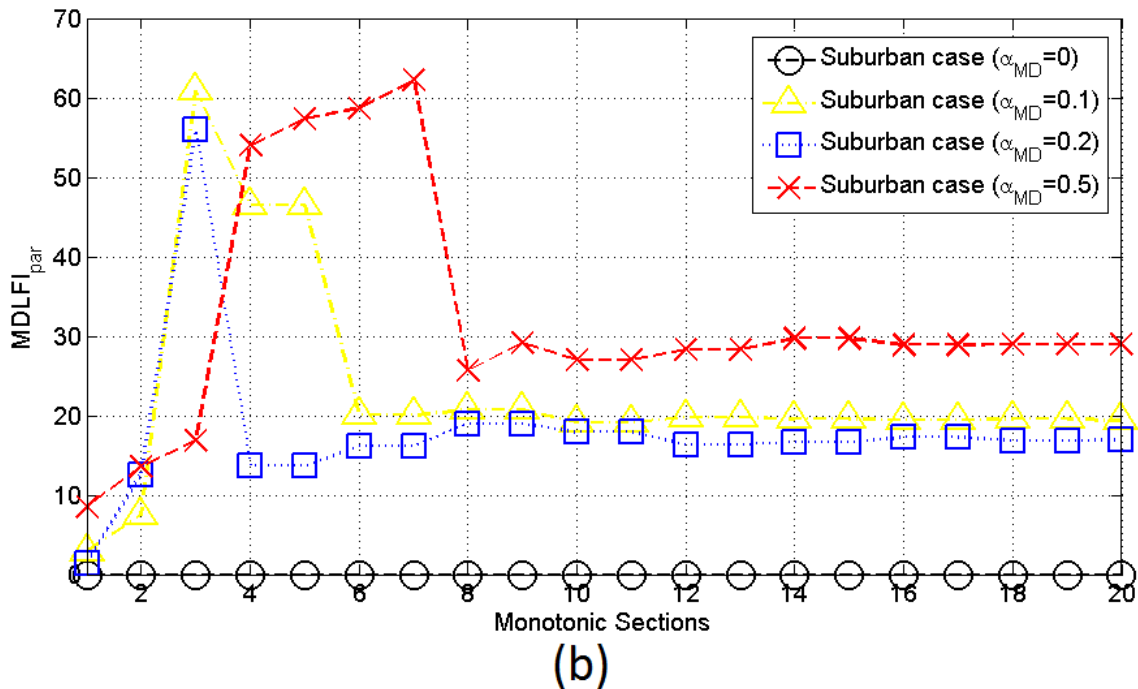
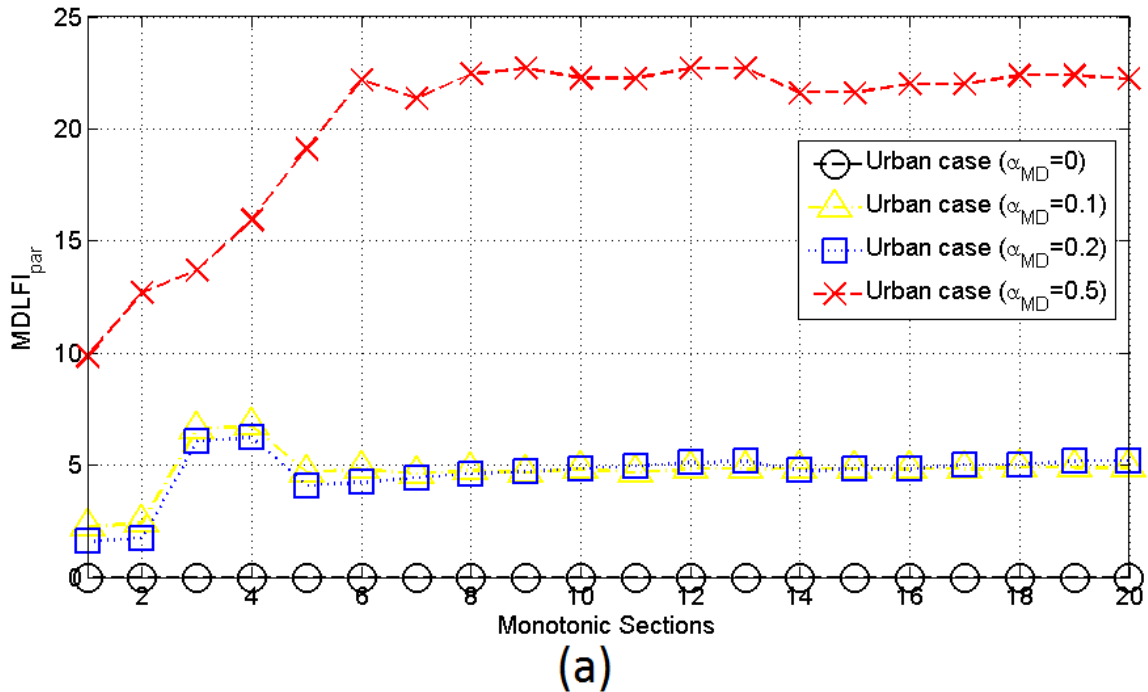
4.3 L1PMA Mitigation of Measurement Differences and $MDLFI_{par}$

Already been presented in Sec. 4.2, measurement differences can create significant deviations between experimental measurements and theoretical results during the determination of OV MV BPL coupling reflection coefficients, thus, creating ambiguity, whether a main distribution line fault or noisy environment occurs. On the basis of [3], [4], piecewise monotonic data approximations, such as L1PMA, L2WPMA and L2CXCVC, achieve to mitigate the additive measurement differences by simply maintaining the monotonicity pattern of each OV MV BPL coupling transfer function. Extending the previous concept, L1PMA is here applied to coupling reflection coefficients so that the mitigation of measurement differences may occur and a robust decision regarding the existence of a main distribution line fault can be supported. Actually, the mitigation performance of L1PMA mainly depends on the magnitude of measurement differences and the applied number of monotonic sections.

In accordance with [3], L1PMA identifies the primary extrema of the examined curves and, then, interpolate the data at these extrema. In the case of L1PMA, which is examined in this paper, the low number of monotonic sections blocks the high fluctuations imposed by the high magnitudes of measurement differences, thus giving a general data approximation that follows the monotonicity pattern. Conversely, when a high number of monotonic sections is adopted, L1PMA very efficiently approximate the curves by following them in the depth and the extent of spectral notches but the data approximation cannot mitigate the measurement differences in that sense. In the last case, L1PMA considers measurement differences as part of the OV MV BPL coupling reflection coefficients.

The proposed MDLFI of eq. (4) tries to overall exploit the result versatility of the application of different number of monotonic sections through $MDLFI_{par}$ of eq. (5) by

considering $k_{\text{sect,min}}$ and $k_{\text{sect,max}}$ to be equal to 1 and 20, respectively. In Fig. 4(a), $\text{MDLFI}_{\text{par}}$ is plotted versus the number of monotonic sections for the indicative theoretical OV MV BPL urban case when the four indicative measurement difference distributions of Sec.4.2 are applied. In Figs. 4(b)-(d), same curves with Fig. 4(a) are presented but for the case of the indicative OV MV BPL suburban, rural and “LOS” case, respectively.



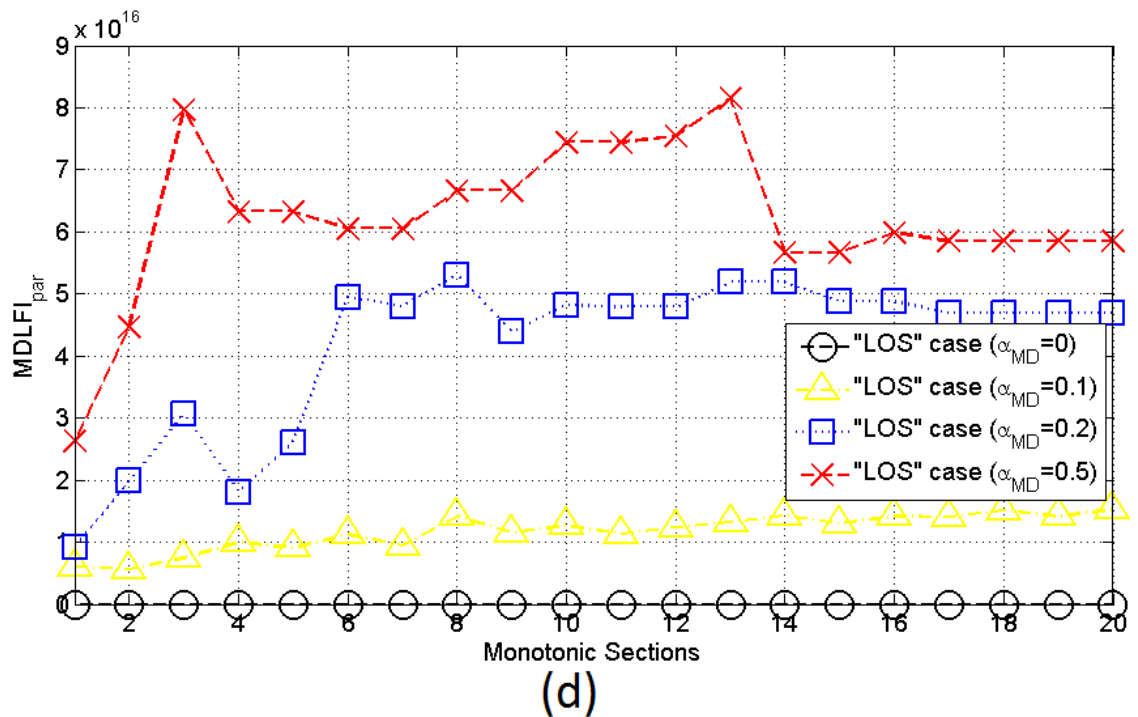
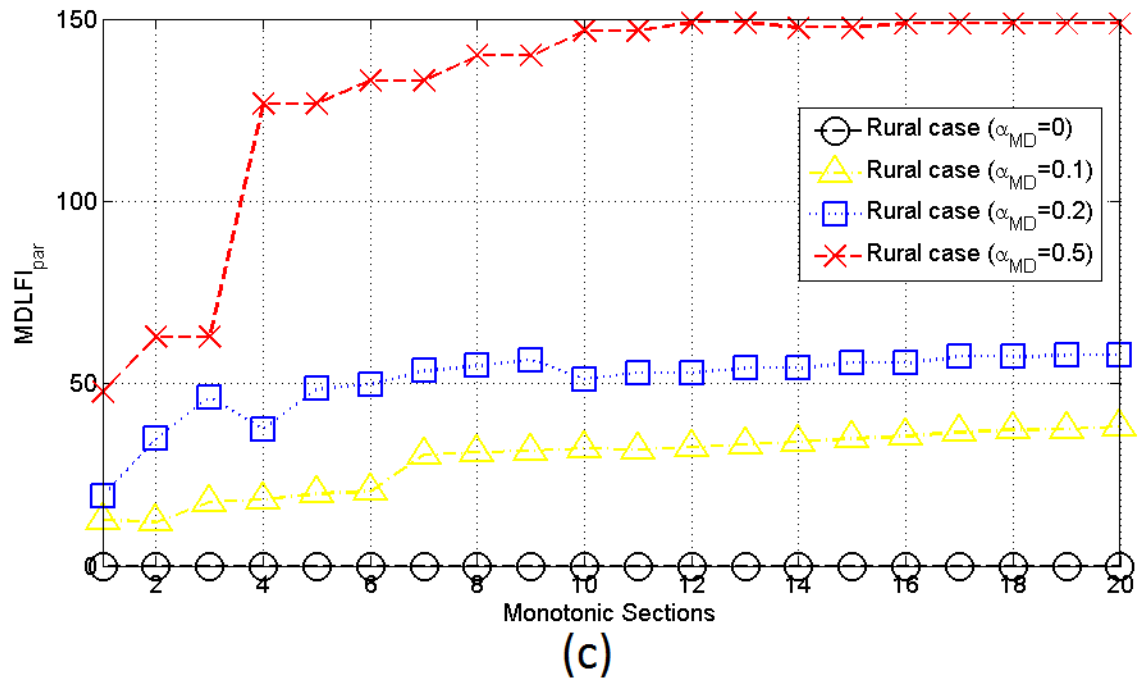
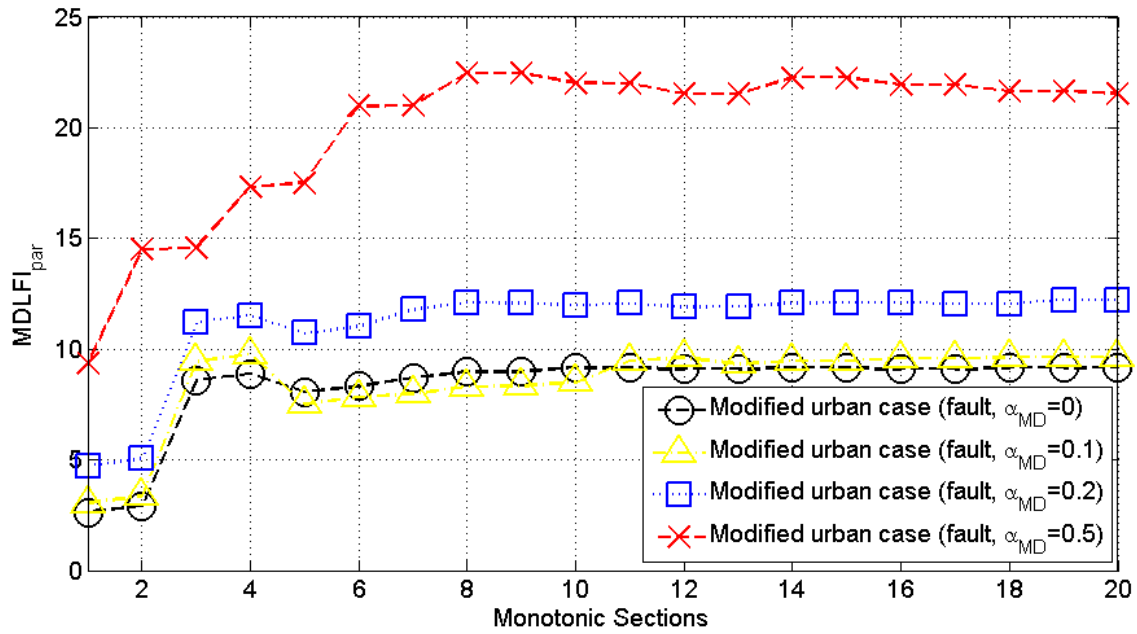


Figure 4. MDLFI_{par} of OV MV BPL topologies contaminated by the four indicative measurement difference distributions (CUD/a_{MD}=0, CUD/a_{MD}=0.1, CUD/a_{MD}=0.2 and CUD/a_{MD}=0.5). (a) Urban case. (b) Suburban case. (c) Rural case. (d) "LOS" case.

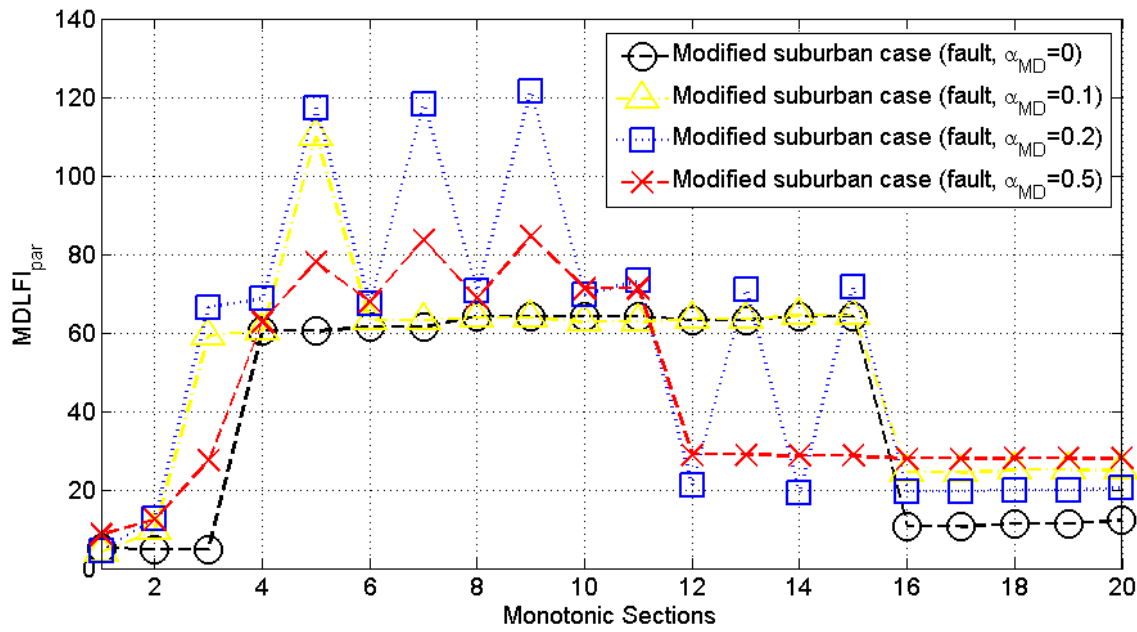
From Figs. 4(a)-(d), it is obvious that MDLFI_{par} uniquely characterizes an OV MV BPL topology however its curve depends on the severity of the imposed measurement differences and the examined OV MV BPL topology. For given OV MV BPL topology, the theoretical coupling reflection coefficient is already known and, thus, MDLFI_{par} is equal to zero when measurement differences are neglected. As the

magnitude a_{MD} of measurement difference CUD increases, $MDLFI_{par}$ differentiates from zero presenting increased values.

The combined impact of measurement differences and main distribution line faults on the OV MV BPL coupling reflection coefficient is also investigated through $MDLFI_{par}$. More specifically, in Figs. 5(a)-(d), $MDLFI_{par}$ is plotted versus the number of monotonic sections for the indicative OV MV BPL topologies, respectively –i.e., urban, suburban, rural and “LOS” case of Sec.4.2–. In each figure, $MDLFI_{par}$ after the main distribution line fault at 750m from the transmitting end is given for the respective modified OV MV BPL topology when measurement differences follow four indicative measurement difference distributions, namely: (i) CUD with $a_{MD}=0$ (no measurement differences); (ii) CUD with $a_{MD}=0.1$; (iii) CUD with $a_{MD}=0.2$; and (iv) CUD with $a_{MD}=0.5$. In Figs. 5(a)-(d), the terminal loads during the fault operation are assumed to be short-circuits. In Figs. 6(a)-(d), same figures with Figs. 5(a)-(d) are shown but for the case of open-circuit terminal loads.



(a)



(b)

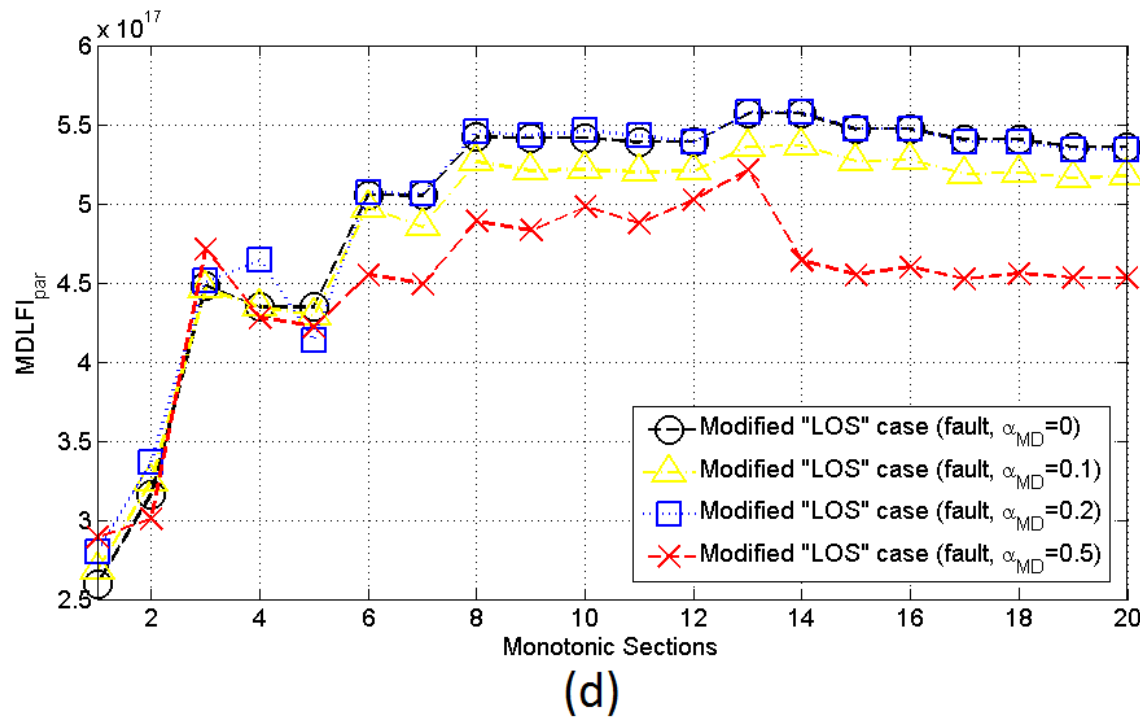
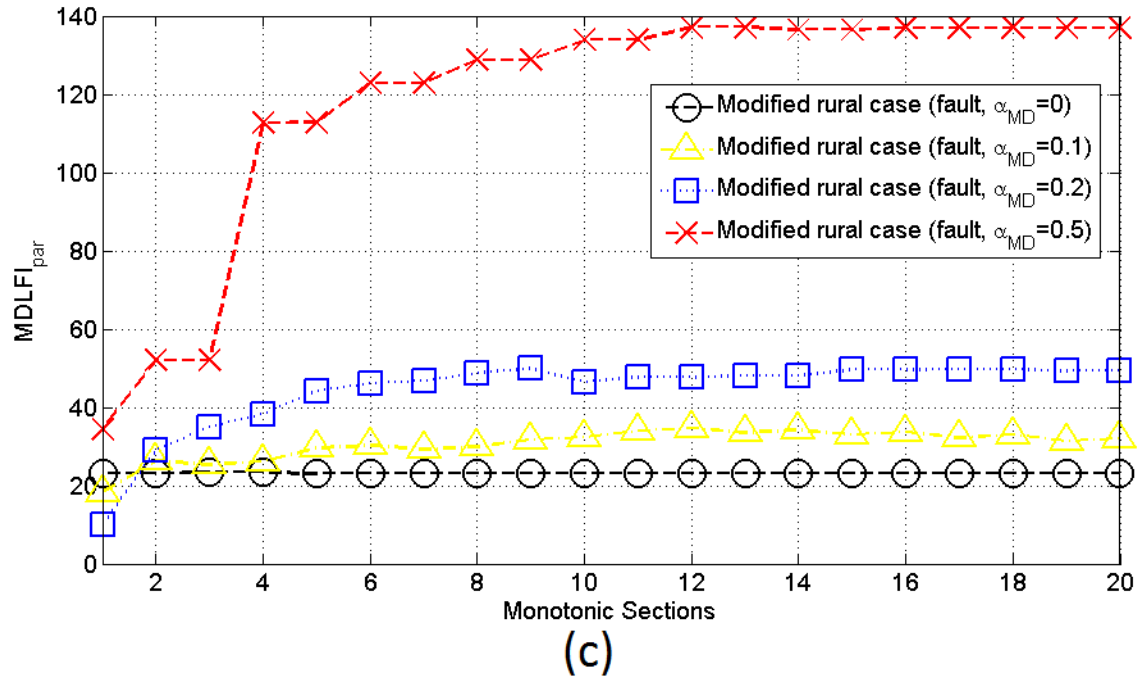
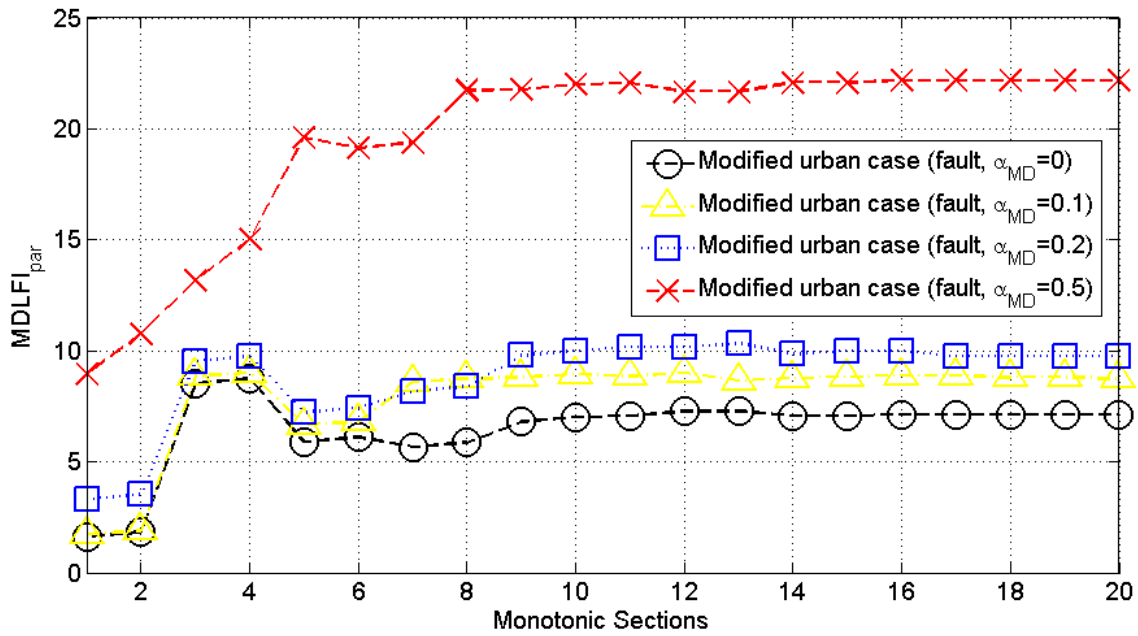
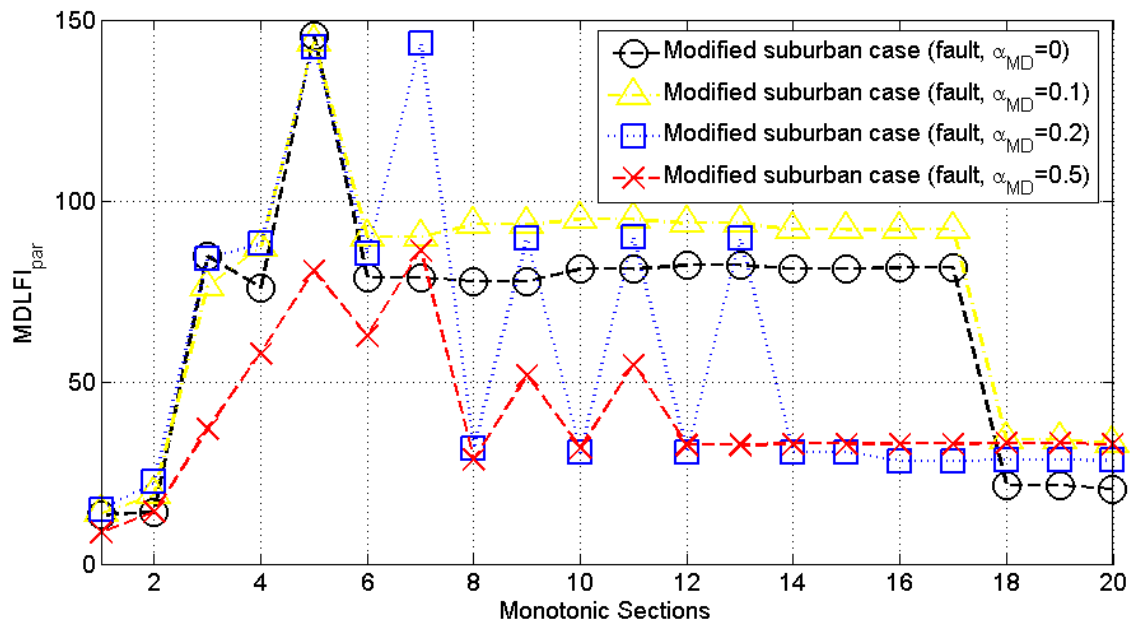


Figure 5. MDLFI_{par} of modified OV MV BPL topologies with short-circuit terminal loads contaminated by the four indicative measurement difference distributions (CUD/a_{MD}=0, CUD/a_{MD}=0.1, CUD/a_{MD}=0.2 and CUD/a_{MD}=0.5). (a) Modified urban case. (b) Modified suburban case. (c) Modified rural case. (d) Modified "LOS" case.



(a)



(b)

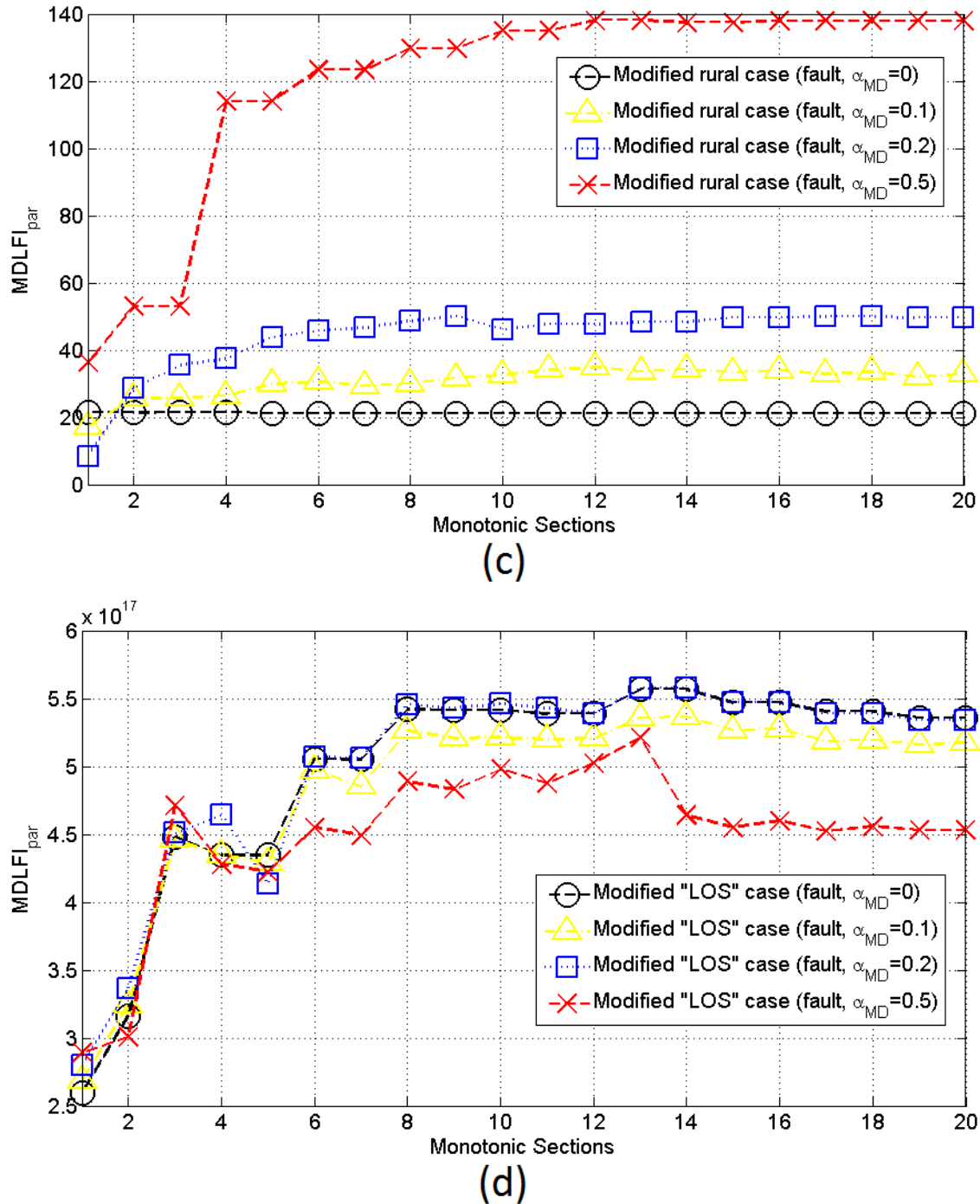
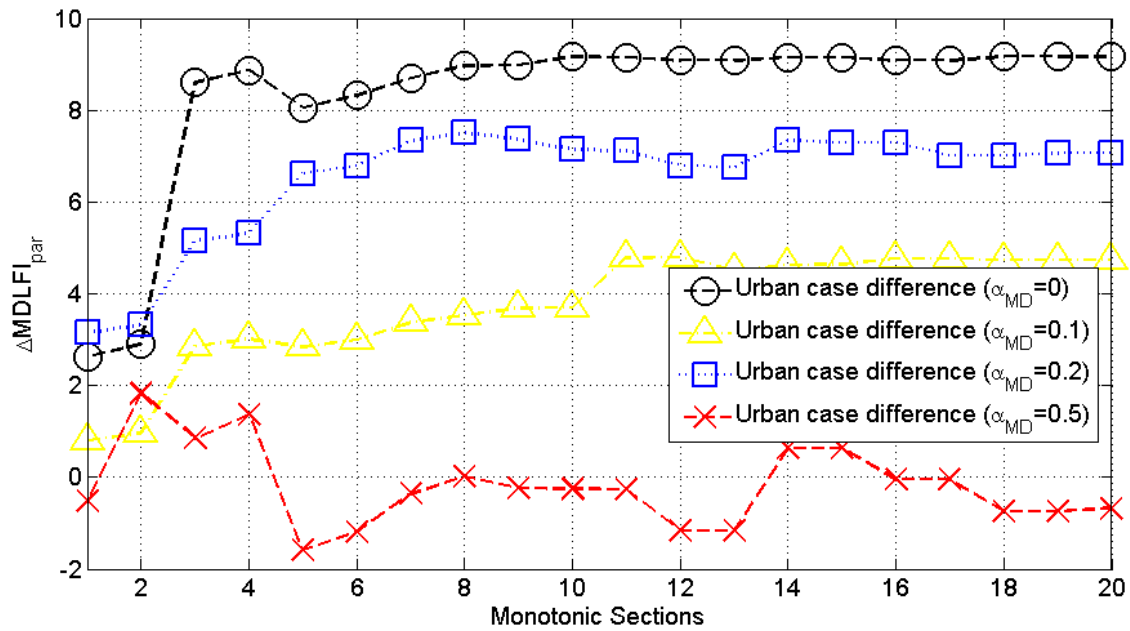


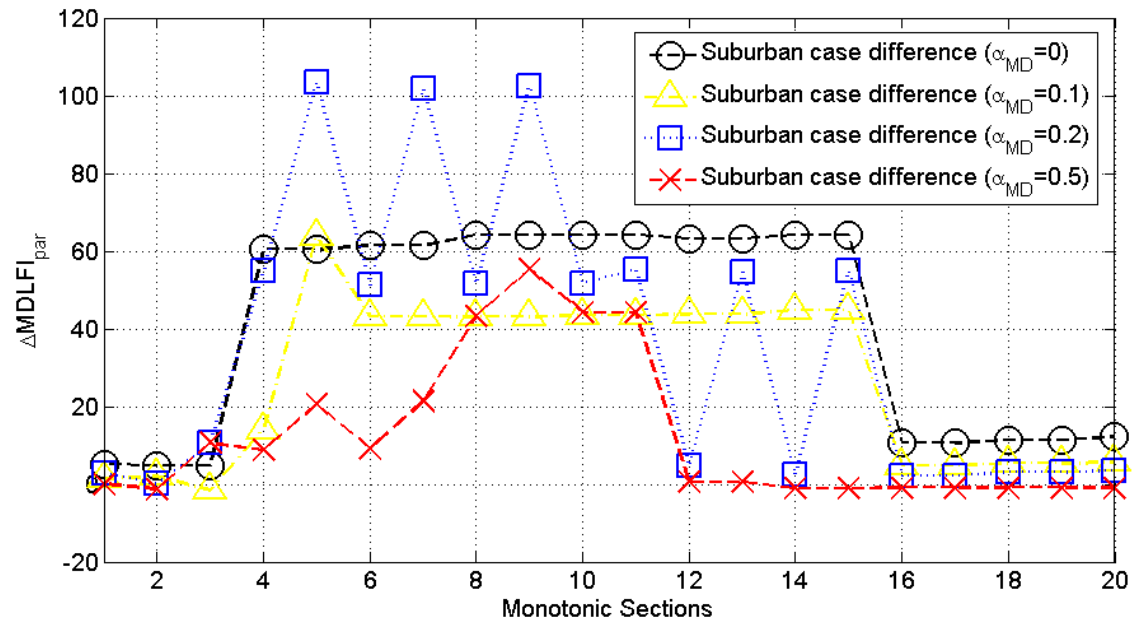
Figure 6. Same plots with Figure 5 but for open-circuit terminal loads during the fault operation.

To facilitate the comparison between Figs 4(a)-(d) with the respective Figs. 5(a)-(d), $\Delta MDLFI_{par}$ that describes the difference between the MDLFI_{par} of modified OV MV BPL topologies and of respective original OV MV BPL topologies is plotted versus the number of monotonic sections in Figs. 7(a)-(d) when short-circuit terminal loads are assumed. In Figs. 8(a)-(d), same curves with Figs. 7(a)-(d) are

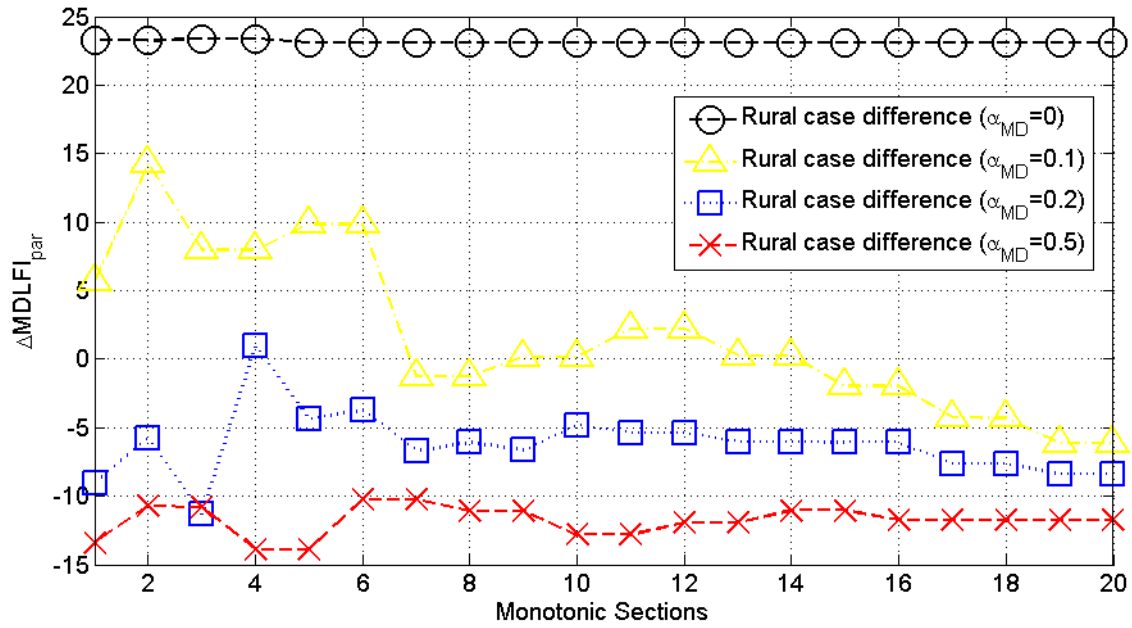
presented but for the case of open-circuit terminal loads; say, the graphical comparison of Figs. 4(a)-(d) with the respective Figs. 6(a)-(d).



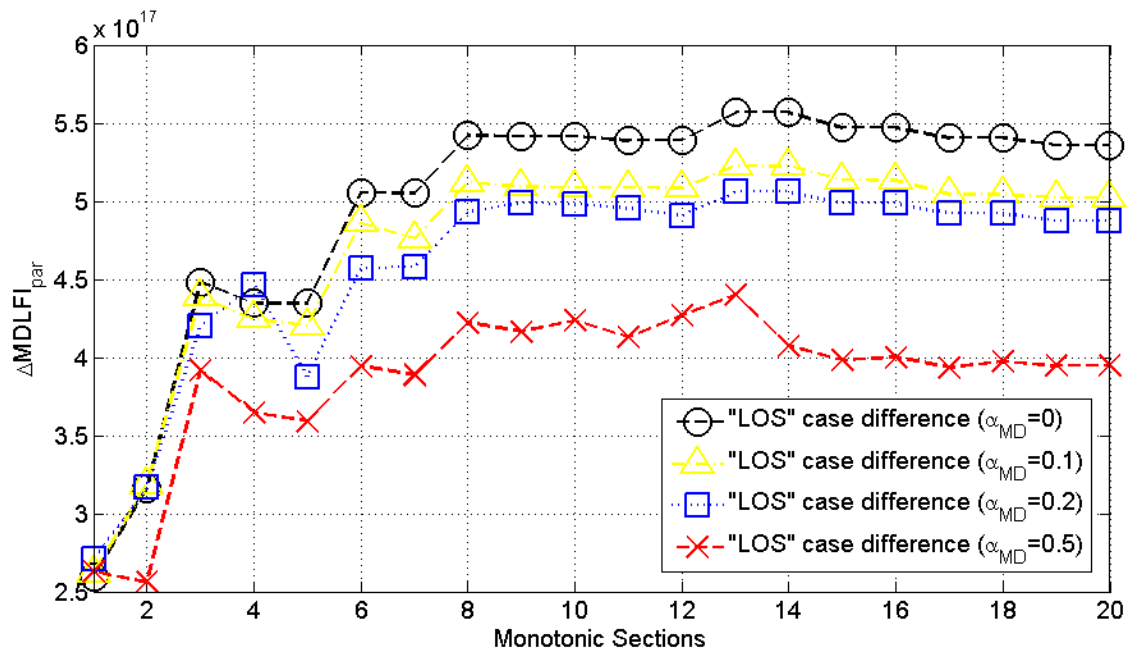
(a)



(b)

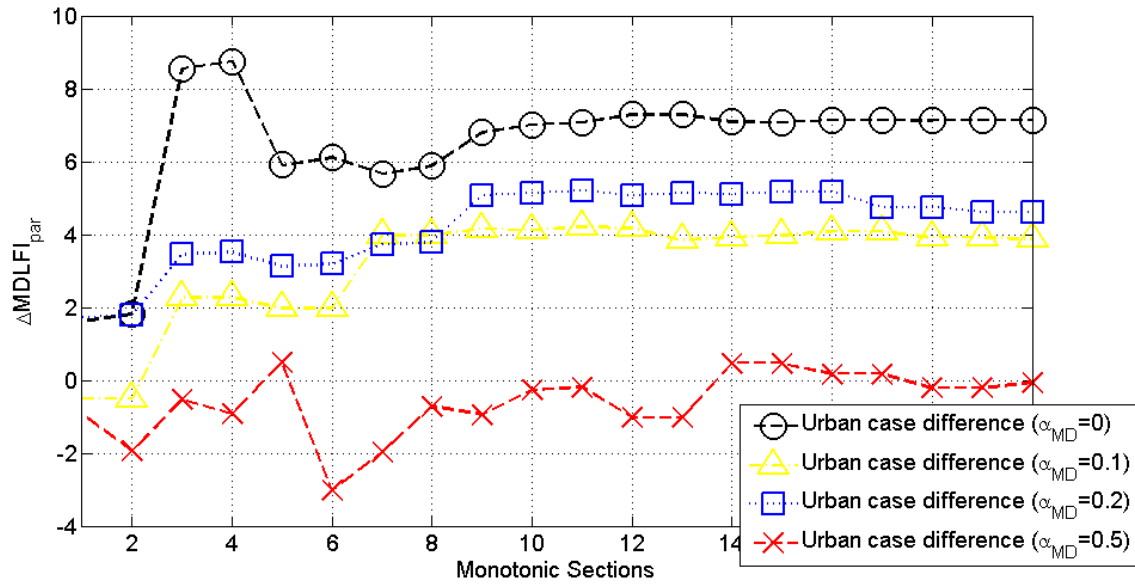


(c)

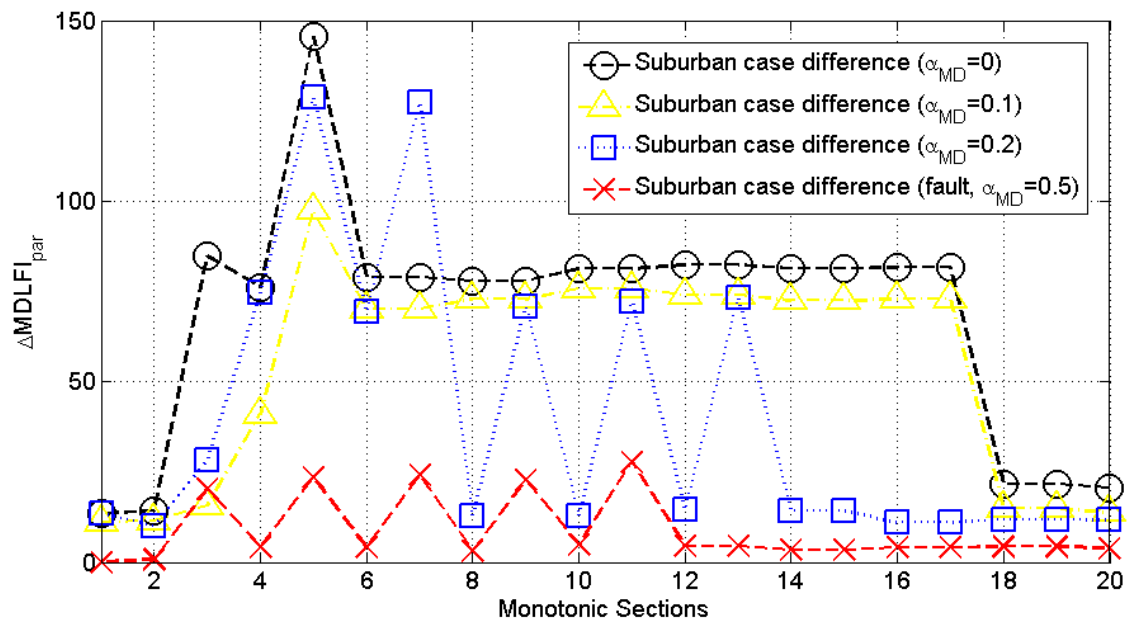


(d)

Figure 7. $\Delta MDLFI_{par}$ between modified OV MV BPL topologies with short-circuit terminal loads and original OV MV BPL topologies when the four indicative measurement difference distributions are applied ($CUD/a_{MD}=0$, $CUD/a_{MD}=0.1$, $CUD/a_{MD}=0.2$ and $CUD/a_{MD}=0.5$). (a) Urban case difference. (b) Suburban case difference. (c) Rural case difference. (d) "LOS" case difference.



(a)



(b)

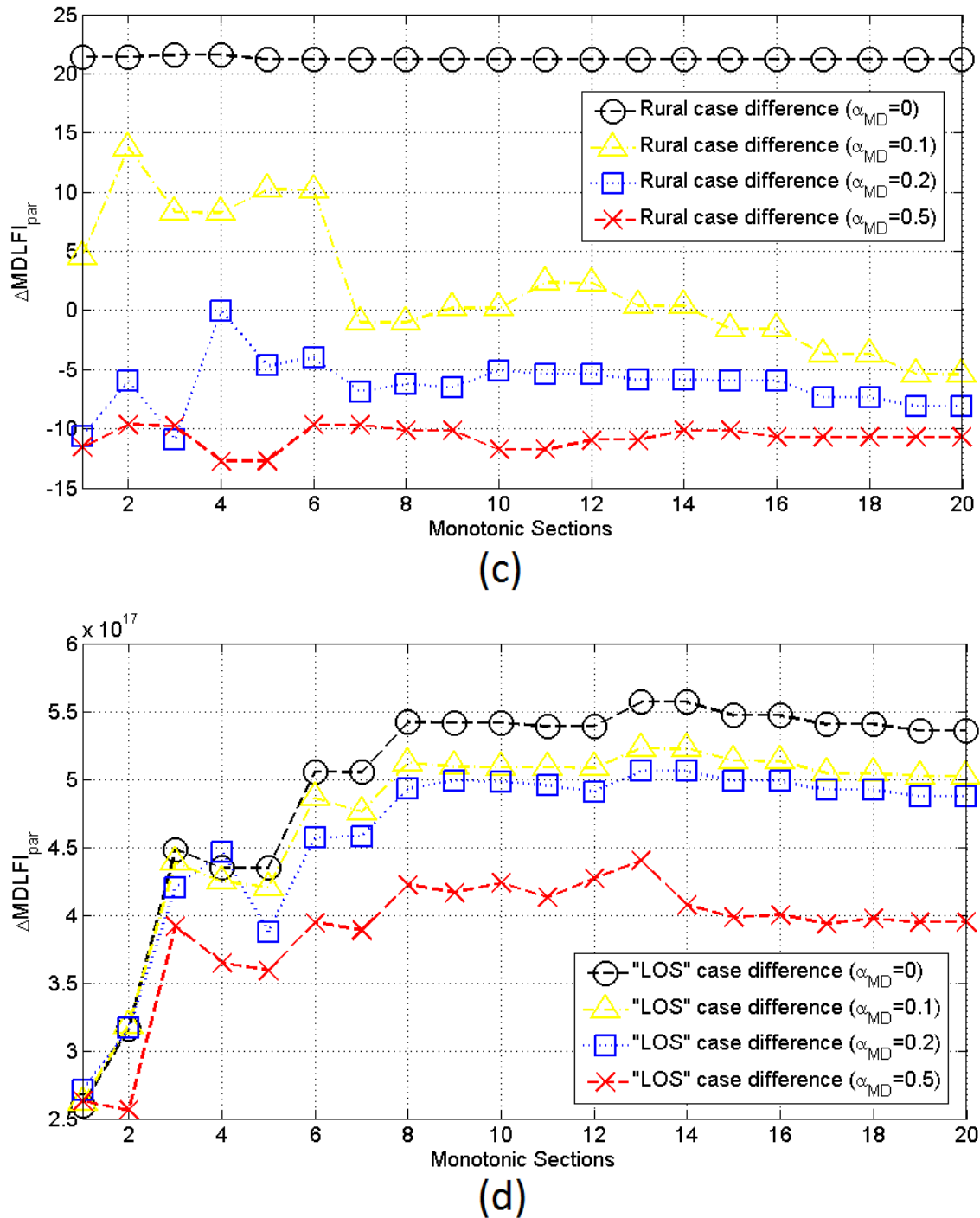


Figure 8. Same plots with Figure 7 but for open-circuit terminal loads during the fault operation.

Comparing Figs. 4(a)-(d), 5(a)-(d), 6(a)-(d), 7(a)-(d) and 8(a)-(d), it is obvious that $\Delta\text{MDLFI}_{\text{par}}$ differences occur between the original and modified OV MV BPL topologies. Although the direct comparison among curves is a difficult task, it is clear that $\Delta\text{MDLFI}_{\text{par}}$ implies the existence of a main distribution line fault when the magnitude a_{MD} of measurement differences is assumed to be equal to zero or remain low (e.g., below 0.1). When the magnitude a_{MD} increases above 0.2 the identification of main

distribution line faults become a precarious venture because it is not clear if the coupling reflection coefficient differences derive from either the modified OV MV BPL topology or the measurement differences. In order to bypass the examination of $MDLFI_{par}$ curves among different OV MV BPL topology cases and quantify the identification problem of main distribution line faults, MDLFI is further calculated in the following subsection. Actually, MDLFI is a derivative performance metric since it is based on $MDLFI_{par}$ of this subsection. Since MDLFI is, in essence, a performance metric similar to the relative error –see eq. (4)–, MDLFI can be straightforward compared to the magnitude a_{MD} of measurement difference distribution.

4.4 MDLFI, MDLFI Thresholds and Decisions Concerning Main Distribution Line Faults in OV MV BPL Topologies

The decision of the existence of a main distribution line fault remains precarious if intense measurement differences should be counteracted during the determination of OV MV BPL coupling reflection coefficients. However, MDLFI that expresses a deviation percentage between the measured and theoretical OV MV BPL coupling reflection coefficients can provide a benchmark result, which further can be compared to the magnitude a_{MD} of the measurement differences taking into account the examined OV MV BPL topology. In this way, MDLFI can support a decision concerning the existence of main distribution line faults. It should be reminded that the original OV MV BPL topologies consist of the four indicative 1000m average path length OV MV BPL topologies whereas modified OV MV BPL topologies, which have been examined until now, comprise the respective original OV MV BPL topologies but for a main distribution line fault that occurs at 750m from the transmitting end by simultaneously implying terminal loads that behave either as short- or open-circuit terminations.

In order to examine the impact of the measurement differences on MDLFI and on relative decisions concerning the existence of faults across the main distribution lines of the examined topologies, MDLFI of the original and modified OV MV BPL topologies of Sec.4.2 is reported in Table 1. MDLFI of Table 1 is investigated when different magnitudes a_{MD} of CUD measurement differences and terminal loads are assumed. Note that the terminal loads of the original OV MV BPL topologies are assumed to be matched to the supported modal characteristic impedances whereas modified OV MV BPL topologies are examined when short- and open-circuit terminations are applied.

By observing the values of Table 1, some interesting remarks can be pointed out, namely:

- From all the columns of MDLFI concerning both original and modified OV MV BPL topologies, it is clear that as the magnitude a_{MD} of CUD measurement differences increases so does MDLFI for given topology, in general.
- Since MDLFI of the original OV MV BPL topologies describes the dissimilarity between the respective theoretical and measured coupling reflection coefficients of original topologies, it is expected that even if small measurement differences get appeared, the coupling reflection coefficient differences of the OV MV BPL topologies with shallow and rare notches (i.e., rural and “LOS” cases) are going to be significantly differentiated. The latter is reflected to high values of MDLFI.

TABLE 1
MDLFI of the Original and Modified OV MV BPL Topologies for Different Magnitudes of Measurement Differences

Magnitude a_{MD} of CUD Measurement Differences	MDLFI											
	Original OV MV BPL Topologies (matched terminal loads)				Modified OV MV BPL Topologies (short-circuit terminal loads)				Modified OV MV BPL Topologies (open-circuit terminal loads)			
	Urban	Suburban	Rural	“LOS”	Urban	Suburban	Rural	“LOS”	Urban	Suburban	Rural	“LOS”
0	0	0	0	0	0.28	1.38	0.77	1.7×10^{16}	0.22	2.28	0.71	1.7×10^{16}
0.1	0.16	0.77	0.96	3.9×10^{14}	0.28	1.67	1.02	1.6×10^{16}	0.26	2.59	1.03	1.6×10^{16}
0.2	0.15	0.59	1.68	1.4×10^{15}	0.37	1.79	1.47	1.7×10^{16}	0.29	1.91	1.47	1.7×10^{16}
0.5	0.67	1.07	4.34	2.1×10^{15}	0.67	1.49	3.95	1.5×10^{16}	0.65	1.35	3.98	1.5×10^{16}

- When a high number of deep spectral notches already occurs in coupling reflection coefficient curves (i.e., curves of original urban and suburban OV MV BPL topologies), the impact of measurement differences on MDLFI is less important in comparison with that of original rural and “LOS” OV MV BPL topologies. Since the spectral notch origin remains unclear, MDLFI values stay low. Therefore, Δ MDLFI between the respective values of original and modified OV MV BPL topologies also remains low implying that harder decision regarding the existence of main distribution line faults could be supported.
- Since the BPL networks are deployed across transmission and distribution networks, theoretical OV MV BPL coupling reflection coefficients and real-time measurements concerning the coupling reflection coefficients can be continuously available. Since theoretical OV MV BPL coupling reflection coefficients are already known for given OV MV BPL topology, an estimation of the magnitude a_{MD} of CUD measurement differences can be achieved by comparing MDLFI of the measured coupling reflection coefficients with the respective theoretical MDLFI values exposed to measurement differences of different magnitudes.

- Real-time measurements of coupling reflection coefficients and an estimation of the magnitude a_{MD} of CUD measurement differences can be easily saved in a database (see MLFLM database of [35]). Since frequent measurements are available and can be retreated right before the main distribution line fault, an estimation of the magnitude a_{MD} of CUD measurement differences can be available at the moment of the appearance of a main distribution line fault. Since measurement differences are not directly affected by the existence of a main distribution line fault, the magnitude a_{MD} of CUD measurement differences that is used during the MDLFI determination can be considered as already known.
- In general terms, the values of the column of MDLFI concerning original OV MV BPL topologies (see grey column of Table 1) can act as the MDLFI threshold for given magnitude a_{MD} of CUD measurement differences and OV MV BPL topology. By observing Table 1, if the grey column values are assumed to be the benchmark metric $MDLFI_{thr}$, the identification of a main distribution line fault is achieved in 26 of 32 cases, say in 81.25%.

To validate the previous findings about the identification of a main distribution line fault through MDLFI, all the possible main distribution line faults that can occur across a given original OV MV BPL topology should be examined for different magnitude a_{MD} of CUD measurement differences. If the previous assertion is valid, MDLFI of the examined OV MV BPL topologies with main distribution line faults should always remain higher than $MDLFI_{thr}$ for given original OV MV BPL topology and magnitude a_{MD} of CUD measurement differences.

Let assume that the identification of a main distribution line fault across the original OV MV BPL urban case is examined. First, the set of all the possible locations of a main distribution line fault should be taken into account when the terminal load is assumed to be either short- or open-circuit termination. In order to create an extended set of possible fault OV MV BPL topologies, the distance of the main distribution line fault from the transmitting end is assumed to be multiples of 50m in this subsection. On the basis of the original OV MV BPL topology, in Fig. 9(a), MDLFI of each possible fault OV MV BPL topology is plotted versus the main distribution line fault distance from the transmitting end when the terminal load is assumed to be short-circuit. MDLFI is computed for the four indicative magnitude a_{MD} of CUD measurement differences that have already been applied in Secs. 4.2 and 4.3. Also, in accordance with the grey column of Table 1, for each magnitude a_{MD} of CUD measurement differences, the respective $MDLFI_{thr}$ is also plotted in Fig. 9(a). Same curves with Fig. 9(a) are given in Fig. 9(b) but for the case of the fault OV MV BPL urban topology with open-circuit termination. In Figs. 10(a) and 10(b), same plots are presented with Figs. 9(a) and 9(b) but for the case of the fault OV MV BPL rural topology.

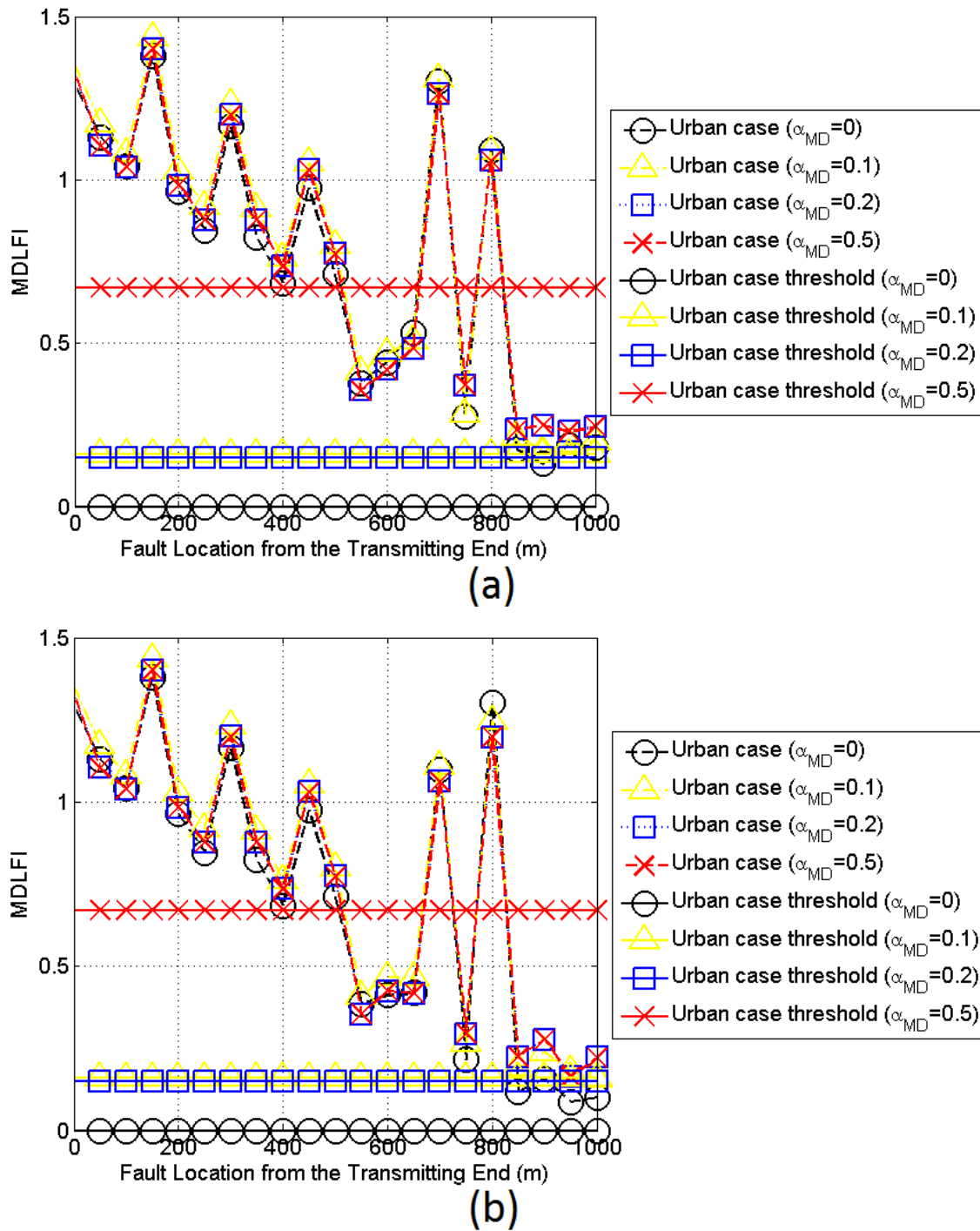


Figure 9. MDLFI of modified OV MV BPL topologies with short-circuit terminal loads and original OV MV BPL topologies when the four indicative measurement difference distributions are applied ($CUD/a_{MD}=0$, $CUD/a_{MD}=0.1$, $CUD/a_{MD}=0.2$ and $CUD/a_{MD}=0.5$). (a) Urban case difference. (b) Suburban case difference. (c) Rural case difference. (d) "LOS" case difference.

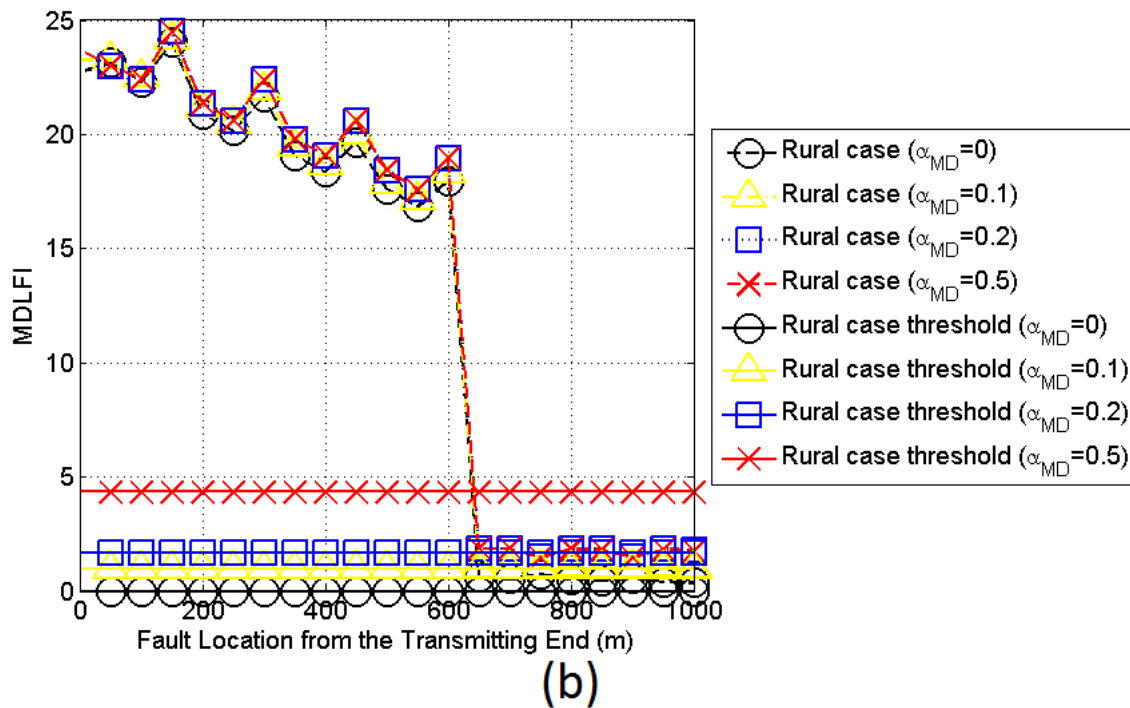
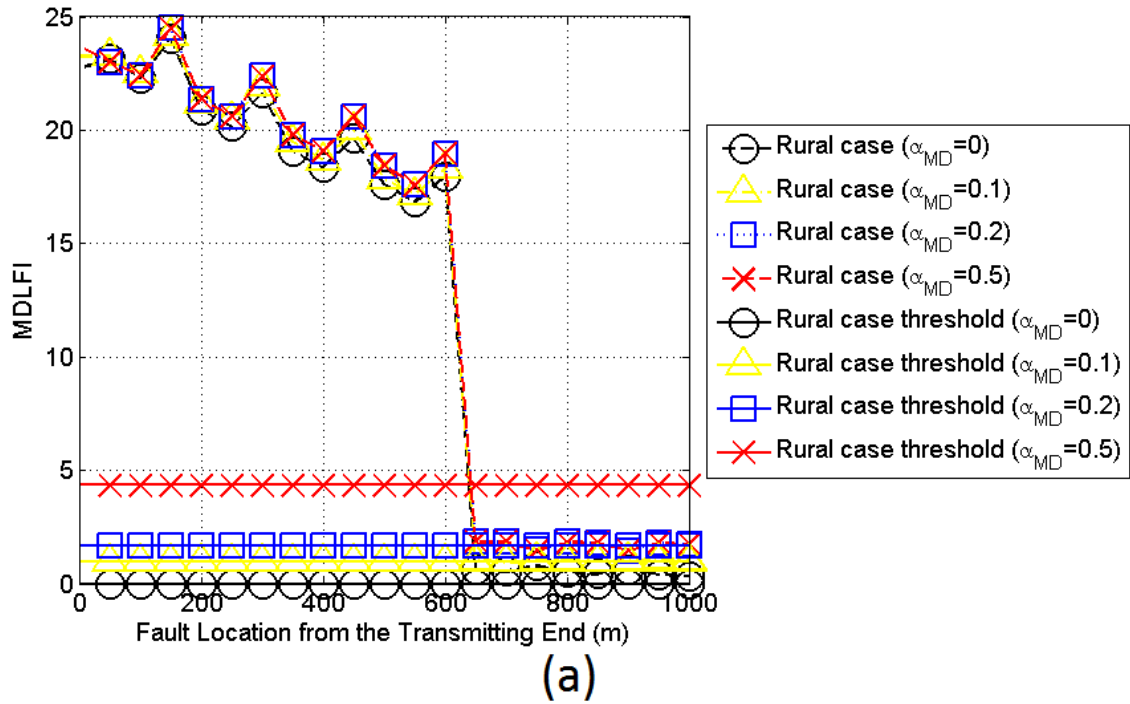


Figure 10. Same plots with Figure 9 but for the identification of main distribution line faults across the original OV MV BPL rural topology.

With reference to Figs. 9(a), 9(b), 10(a) and 10(b), several interesting conclusions concerning the application of MDLFI as well as the corresponding decisions about the identification of a main distribution line fault across the OV MV BPL topologies can be pointed out, namely:

- Already been mentioned in this subsection, MDLFI strongly depends on the examined OV MV BPL topology since it is considered as a dissimilarity metric between the original and fault case. This explains the fact that MDLFI values of fault rural OV MV BPL topologies always remain higher than the ones of fault urban OV MV BPL topologies.
- MDLFI slightly depends on the terminal load of the examined fault OV MV BPL topology. In fact, coupling reflection coefficient differences can be observed when the terminal load is assumed to be equal to short- or open-circuit termination. However, the coupling reflection coefficients for given OV MV BPL topology when terminal loads vary from short- to open-circuit remain low implying low differences between the respective MDLFIs. Hence, apart from the identification of a main distribution line fault, a first idea regarding the nature of the fault and thus the type of the main distribution line fault (day, fault line in the air or on the ground) can be given.
- MDLFI strongly depends on the location of the main distribution line fault across the OV MV BPL topology. In fact, when the fault is located near to the transmitting end, MDLFI receives higher values in comparison with the respective ones of a main distribution line fault located near to the receiving end. Since the identification of the fault is achieved through the comparison of MDLFI of the fault OV MV BPL topology against the $MDLFI_{thr}$ of the original one, this implies that the identification of a main distribution line fault becomes easier when it is located near to the transmitting end than far away from it. This is a logical result since the fault OV MV BPL topology is critically modified in comparison with the original one when the fault is near to the transmitting end. Not only the overall transmission length of the fault OV MV BPL topology becomes lower than the average length of 1000m but a number of branches can be omitted in the fault OV MV BPL topology. In order to cope with this fault location sensitivity, MLFLM exploits MDLFI measurements of both the available sides of an OV MV BPL topology –say, transmitting and receiving end– (for more details concerning the combined MLFLM application of MDLFI, see [35]).
- Already been recognized from Table 1, as the magnitude a_{MD} of measurement differences increases so does the difficulty of identifying a main distribution line fault. This can be explained by the fact that the magnitude increase of measurement differences creates an increase to $MDLFI_{thr}$ that anyway defines the critical line between the normal and fault operation. As $MDLFI_{thr}$ increases, the distinction between the normal and fault condition becomes problematic. From the Figures, it is clear that MDLFI of the examined OV MV BPL topologies always remains above $MDLFI_{thr}$ when magnitudes a_{MD} of measurement differences remain low (e.g., $a_{MD}=0$ and $a_{MD}=0.1$). In these cases of low measurement differences, the difference between MDLFI and $MDLFI_{thr}$ remains large enough so that a robust decision regarding the existence of a main distribution line fault can be supported. Conversely, when magnitudes a_{MD} of

measurement differences start to get high, the difference between MDLFI and $MDLFI_{thr}$ diminishes, thus confusing and creating a decision ambiguity whether a main distribution line fault exists. Marginally, when the magnitude a_{MD} of measurement differences is equal to 0.5, the decision of the existence of a main distribution line fault becomes critically uncertain. Numerically, in all the four OV MV BPL topologies examined in Figs. 9(a), 9(b), 10(a) and 10(b), although a main distribution line fault occurs, a safe decision concerning this existence cannot be safely supported in 8 of the 20 cases when the magnitude a_{MD} of the measurement differences is assumed to be equal to 0.5. Here, it should be noted that all the 8 problematic main distribution line fault cases are situated near to the receiving end, which is a problematic condition for a single MDLFI measurement from the transmitting end, as already been mentioned.

The identification of main distribution line faults in OV MV BPL topologies regardless of the presence of measurement differences and the nature of the terminal load concludes the main prerequisite of applying MLFLM. Since the existence of main distribution line faults can be secured with a high degree of accuracy, the next phase of MLFLM that is the exact localization of the fault across the examined OV MV BPL topology is analyzed in [35].

5. Conclusions

The main distribution line fault identification methodology of the first paper has further been extended in this paper so that measurement differences of the coupling reflection coefficients can be mitigated. Through the application of LIPMA and its accompanying metrics, such as $MDLFI_{par}$, MDLFI and $MDLFI_{thr}$, a secure identification of a main distribution line fault across the OV MV BPL networks can be achieved when magnitude a_{MD} of measurement differences that follow CUD remains low or normal (i.e., a_{MD} lower than 0.2). In the vast majority of the cases examined, the decision regarding the fault identification remains robust when magnitude a_{MD} remains, indeed, low or normal. In contrast, when the magnitude a_{MD} of measurement differences becomes significant and comparable to the depth of the spectral notches of the coupling reflection coefficients (i.e., a_{MD} higher than 0.2), decisions regarding the existence of main distribution line fault become insecure especially when the faults are situated near to the receiving end, far away from the measurement site. Anyway, the decision regarding the identification of main distribution line faults are considered to be more reliable when the faults are located near to the transmitting end of the examined OV MV BPL topologies.

The combined operation of extended TM2 method, LIPMA and set of MDLFI-related metrics concludes the introductory phase of MLFLM. However, the main phase of MLFLM that has to do with the exact localization of main distribution line faults across the OV MV BPL topologies is analyzed in the third paper.

CONFLICTS OF INTEREST

The author declares that there is no conflict of interests regarding the publication of this paper.

References

- [1] A. G. Lazaropoulos, "Main Line Fault Localization Methodology in Smart Grid – Part 1: Extended TM2 Method for the Overhead Medium-Voltage Broadband over Power Lines Networks Case," *Trends in Renewable Energy*, vol. 3, no. 3, pp. 2-25, 2017.
- [2] A. G. Lazaropoulos, A. Sarafi, and P. G. Cottis, "The emerging smart grid — A pilot MV/BPL network installed at Lavrion, Greece," in *Proc. Workshop on Applications for Powerline Communications WSPLC 2008*, Thessaloniki, Greece, Oct. 2008. [Online]. Available: http://newton.ee.auth.gr/WSPLC08/Abstracts%5CSG_3.pdf
- [3] A. G. Lazaropoulos, "Power Systems Stability through Piecewise Monotonic Data Approximations – Part 1: Comparative Benchmarking of L1PMA, L2WPMA and L2CXCVC in Overhead Medium-Voltage Broadband over Power Lines Networks," *Trends in Renewable Energy*, vol. 3, no. 1, pp. 2 – 32, Jan. 2017. [Online]. Available: <http://futureenergysp.com/index.php/tre/article/view/29/34>
- [4] A. G. Lazaropoulos, "Power Systems Stability through Piecewise Monotonic Data Approximations – Part 2: Adaptive Number of Monotonic Sections and Performance of L1PMA, L2WPMA and L2CXCVC in Overhead Medium-Voltage Broadband over Power Lines Networks," *Trends in Renewable Energy*, vol. 3, no. 1, pp. 33 – 60, Jan. 2017. [Online]. Available: <http://futureenergysp.com/index.php/tre/article/view/30/35>
- [5] A. G. Lazaropoulos, "Improvement of Power Systems Stability by Applying Topology Identification Methodology (TIM) and Fault and Instability Identification Methodology (FIIM) – Study of the Overhead Medium-Voltage Broadband over Power Lines (OV MV BPL) Networks Case," *Trends in Renewable Energy*, vol. 3, no. 2, pp. 102 – 128, Apr. 2017. [Online]. Available: <http://futureenergysp.com/index.php/tre/article/view/34/pdf>
- [6] A. G. Lazaropoulos, "Measurement Differences, Faults and Instabilities in Intelligent Energy Systems – Part 1: Identification of Overhead High-Voltage Broadband over Power Lines Network Topologies by Applying Topology Identification Methodology (TIM)," *Trends in Renewable Energy*, vol. 2, no. 3, pp. 85 – 112, Oct. 2016.
- [7] A. G. Lazaropoulos and P. Lazaropoulos, "Financially Stimulating Local Economies by Exploiting Communities' Microgrids: Power Trading and Hybrid Techno-Economic (HTE) Model," *Trends in Renewable Energy*, vol. 1, no. 3, pp. 131-184, Sep. 2015. [Online]. Available: <http://futureenergysp.com/index.php/tre/article/view/14>
- [8] L. Lutz, A. M. Tonello, and T. G. Swart, *Power Line Communications: Principles, Standards and Applications from multimedia to smart grid*, John Wiley & Sons, 2016.
- [9] G. Artale, A. Cataliotti, V. Cosentino, D. Di Cara, R. Fiorelli, S. Guaiana, and G. Tine, "A New Low Cost Coupling System for Power Line Communication on Medium Voltage Smart grids," *IEEE Trans. on Smart Grid*, to be published, 2017.
- [10] A. G. Lazaropoulos, "Measurement Differences, Faults and Instabilities in Intelligent Energy Systems – Part 2: Fault and Instability Prediction in Overhead High-Voltage Broadband over Power Lines Networks by Applying Fault and

- Instability Identification Methodology (FIIM),” *Trends in Renewable Energy*, vol. 2, no. 3, pp. 113 – 142, Oct. 2016. [Online]. Available: <http://futureenergysp.com/index.php/tre/article/view/27/33>
- [11] A. G. Lazaropoulos, “Factors Influencing Broadband Transmission Characteristics of Underground Low-Voltage Distribution Networks,” *IET Commun.*, vol. 6, no. 17, pp. 2886-2893, Nov. 2012.
- [12] A. G. Lazaropoulos and P. G. Cottis, “Transmission characteristics of overhead medium voltage power line communication channels,” *IEEE Trans. Power Del.*, vol. 24, no. 3, pp. 1164-1173, Jul. 2009.
- [13] A. G. Lazaropoulos and P. G. Cottis, “Capacity of overhead medium voltage power line communication channels,” *IEEE Trans. Power Del.*, vol. 25, no. 2, pp. 723-733, Apr. 2010.
- [14] A. G. Lazaropoulos and P. G. Cottis, “Broadband transmission via underground medium-voltage power lines-Part I: transmission characteristics,” *IEEE Trans. Power Del.*, vol. 25, no. 4, pp. 2414-2424, Oct. 2010.
- [15] A. G. Lazaropoulos and P. G. Cottis, “Broadband transmission via underground medium-voltage power lines-Part II: capacity,” *IEEE Trans. Power Del.*, vol. 25, no. 4, pp. 2425-2434, Oct. 2010.
- [16] A. G. Lazaropoulos, “Broadband transmission characteristics of overhead high-voltage power line communication channels,” *Progress in Electromagnetics Research B*, vol. 36, pp. 373-398, 2012. [Online]. Available: <http://www.jpier.org/PIERB/pierb36/19.11091408.pdf>
- [17] A. G. Lazaropoulos, “Towards broadband over power lines systems integration: Transmission characteristics of underground low-voltage distribution power lines,” *Progress in Electromagnetics Research B*, 39, pp. 89-114, 2012. [Online]. Available: <http://www.jpier.org/PIERB/pierb39/05.12012409.pdf>
- [18] A. G. Lazaropoulos, “Broadband transmission and statistical performance properties of overhead high-voltage transmission networks,” *Hindawi Journal of Computer Networks and Commun.*, 2012, article ID 875632, 2012. [Online]. Available: <http://www.hindawi.com/journals/jcnc/aip/875632/>
- [19] A. G. Lazaropoulos, “Towards modal integration of overhead and underground low-voltage and medium-voltage power line communication channels in the smart grid landscape: model expansion, broadband signal transmission characteristics, and statistical performance metrics (Invited Paper),” *ISRN Signal Processing*, vol. 2012, Article ID 121628, 17 pages, 2012. [Online]. Available: <http://www.isrn.com/journals/sp/aip/121628/>
- [20] A. G. Lazaropoulos, “Review and Progress towards the Common Broadband Management of High-Voltage Transmission Grids: Model Expansion and Comparative Modal Analysis,” *ISRN Electronics*, vol. 2012, Article ID 935286, pp. 1-18, 2012. [Online]. Available: <http://www.hindawi.com/isrn/electronics/2012/935286/>
- [21] A. G. Lazaropoulos, “Review and Progress towards the Capacity Boost of Overhead and Underground Medium-Voltage and Low-Voltage Broadband over Power Lines Networks: Cooperative Communications through Two- and Three-Hop Repeater Systems,” *ISRN Electronics*, vol. 2013, Article ID 472190, pp. 1-19, 2013. [Online]. Available: <http://www.hindawi.com/isrn/electronics/aip/472190/>
- [22] A. G. Lazaropoulos, “Green Overhead and Underground Multiple-Input Multiple-Output Medium Voltage Broadband over Power Lines Networks: Energy-

- Efficient Power Control,” *Springer Journal of Global Optimization*, vol. 2012 / Print ISSN 0925-5001, pp. 1-28, Oct. 2012.
- [23] P. Amirshahi and M. Kavehrad, “High-frequency characteristics of overhead multiconductor power lines for broadband communications,” *IEEE J. Sel. Areas Commun.*, vol. 24, no. 7, pp. 1292-1303, Jul. 2006.
- [24] T. Sartenaer, “Multiuser communications over frequency selective wired channels and applications to the powerline access network” Ph.D. dissertation, Univ. Catholique Louvain, Louvain-la-Neuve, Belgium, Sep. 2004. [Online] Available: https://dial.uclouvain.be/pr/boreal/en/object/boreal%3A5010/datastream/PDF_12/view
- [25] T. Calliacoudas and F. Issa, ““Multiconductor transmission lines and cables solver,” An efficient simulation tool for plc channel networks development,” presented at the *IEEE Int. Conf. Power Line Communications and Its Applications*, Athens, Greece, Mar. 2002.
- [26] A. G. Lazaropoulos, “Best L1 Piecewise Monotonic Data Approximation in Overhead and Underground Medium-Voltage and Low-Voltage Broadband over Power Lines Networks: Theoretical and Practical Transfer Function Determination,” *Hindawi Journal of Computational Engineering*, vol. 2016, Article ID 6762390, 24 pages, 2016. doi:10.1155/2016/6762390. [Online]. Available: <https://www.hindawi.com/journals/jcengi/2016/6762390/cta/>
- [27] P. Amirshahi, “Broadband access and home networking through powerline networks” Ph.D. dissertation, Pennsylvania State Univ., University Park, PA, May 2006. [Online]. Available: <http://etda.libraries.psu.edu/theses/approved/WorldWideIndex/ETD-1205/index.html>
- [28] M. D’Amore and M. S. Sarto, “Simulation models of a dissipative transmission line above a lossy ground for a wide-frequency range-Part I: Single conductor configuration,” *IEEE Trans. Electromagn. Compat.*, vol. 38, no. 2, pp. 127-138, May 1996.
- [29] M. D’Amore and M. S. Sarto, “Simulation models of a dissipative transmission line above a lossy ground for a wide-frequency range-Part II: Multi-conductor configuration,” *IEEE Trans. Electromagn. Compat.*, vol. 38, no. 2, pp. 139-149, May 1996.
- [30] A. Milioudis, G. T. Andreou, and D. P. Labridis, “Detection and location of high impedance faults in multiconductor overhead distribution lines using power line communication devices,” *IEEE Trans. on Smart Grid*, vol. 6, no. 2, pp. 894-902, 2015.
- [31] A. G. Lazaropoulos, “Designing Broadband over Power Lines Networks Using the Techno-Economic Pedagogical (TEP) Method – Part I: Overhead High Voltage Networks and Their Capacity Characteristics,” *Trends in Renewable Energy*, vol. 1, no. 1, pp. 16-42, Mar. 2015. [Online]. Available: <http://futureenergysp.com/index.php/tre/article/view/2>
- [32] A. G. Lazaropoulos, “Designing Broadband over Power Lines Networks Using the Techno-Economic Pedagogical (TEP) Method – Part II: Overhead Low-Voltage and Medium-Voltage Channels and Their Modal Transmission Characteristics,” *Trends in Renewable Energy*, vol. 1, no. 2, pp. 59-86, Jun. 2015. [Online]. Available: <http://futureenergysp.com/index.php/tre/article/view/6/16>

- [33] T. Sartenaer and P. Delogne, “Deterministic modelling of the (Shielded) outdoor powerline channel based on the multiconductor transmission line equations,” *IEEE J. Sel. Areas Commun.*, vol. 24, no. 7, pp. 1277-1291, Jul. 2006.
- [34] <http://cpc.cs.qub.ac.uk/summaries/ADRF>
- [35] A. G. Lazaropoulos, “Main Line Fault Localization Methodology in Smart Grid – Part 3: Main Line Fault Localization Methodology (MLFLM),” *Trends in Renewable Energy*, vol. 3, no. 3, pp. 62-81, 2017.

Article copyright: © 2017 Athanasios G. Lazaropoulos.



This work is licensed under a [Creative Commons Attribution 4.0 International License](https://creativecommons.org/licenses/by/4.0/).